





STAT1 Contributes to Microglial/Macrophage Inflammation and Neurological Dysfunction in a Mouse Model of Traumatic Brain Injury

 Yongfang Zhao,^{1*} Cheng Ma,^{1*} Caixia Chen,¹ Sicheng Li,¹ Yangfan Wang,¹ Tuo Yang,^{1,2} R. Anne Stetler,^{1,2} Michael V. L. Bennett,³  C. Edward Dixon,^{2,4}  Jun Chen,^{1,2} and  Yejie Shi^{1,2}

¹Pittsburgh Institute of Brain Disorders & Recovery and Department of Neurology, University of Pittsburgh, Pittsburgh, Pennsylvania 15213,

²Geriatric Research, Education and Clinical Center, Veterans Affairs Pittsburgh Health Care System, Pittsburgh, Pennsylvania 15261, ³Dominick P. Purpura Department of Neuroscience, Albert Einstein College of Medicine, Bronx, New York 10461, and ⁴Department of Neurosurgery, University of Pittsburgh, Pittsburgh, Pennsylvania 15213

Traumatic brain injury (TBI) triggers a plethora of inflammatory events in the brain that aggravate secondary injury and impede tissue repair. Resident microglia (Mi) and blood-borne infiltrating macrophages (MΦ) are major players of inflammatory responses in the post-TBI brain and possess high functional heterogeneity. However, the plasticity of these cells has yet to be exploited to develop therapies that can mitigate brain inflammation and improve the outcome after TBI. This study investigated the transcription factor STAT1 as a key determinant of proinflammatory Mi/MΦ responses and aimed to develop STAT1 as a novel therapeutic target for TBI using a controlled cortical impact model of TBI on adult male mice. TBI induced robust upregulation of STAT1 in the brain at the subacute injury stage, which occurred primarily in Mi/MΦ. Intraperitoneal administration of fludarabine, a selective STAT1 inhibitor, markedly alleviated proinflammatory Mi/MΦ responses and brain inflammation burden after TBI. Such phenotype-modulating effects of fludarabine on post-TBI Mi/MΦ were reproduced by tamoxifen-induced, selective KO of STAT1 in Mi/MΦ (STAT1 mKO). By propelling Mi/MΦ away from a detrimental proinflammatory phenotype, STAT1 mKO was sufficient to reduce long-term neurologic deficits and brain lesion size after TBI. Importantly, short-term fludarabine treatment after TBI elicited long-lasting improvement of TBI outcomes, but this effect was lost on STAT1 mKO mice. Together, our study provided the first line of evidence that STAT1 causatively determines the proinflammatory phenotype of brain Mi/MΦ after TBI. We also showed promising preclinical data supporting the use of fludarabine as a novel immunomodulating therapy to TBI.

Key words: behavioral test; conditional gene KO; controlled cortical impact; fludarabine; neuroinflammation; signal transducer and activator of transcription 1

Significance Statement

The functional phenotype of microglia and macrophages (Mi/MΦ) critically influences brain inflammation and the outcome after traumatic brain injury (TBI); however, no therapies have been developed to modulate Mi/MΦ functions to treat TBI. Here we report, for the first time, that the transcription factor STAT1 is a key mediator of proinflammatory Mi/MΦ responses in the post-TBI brain, the specific deletion of which ameliorates neuroinflammation and improves long-term functional recovery after TBI. We also show excellent efficacy of a selective STAT1 inhibitor fludarabine against TBI-induced functional deficits and brain injury using a mouse model, presenting STAT1 as a promising therapeutic target for TBI.

Received Mar. 30, 2022; revised June 29, 2022; accepted Aug. 15, 2022.

Author contributions: Y.Z., C.M., C.C., S.L., Y.W., T.Y., and Y.S. performed research; Y.Z., C.M., C.C., S.L., Y.W., T.Y., and Y.S. analyzed data; Y.Z., R.A.S., M.V.L.B., C.E.D., and J.C. edited the paper; J.C. and Y.S. designed research; Y.S. wrote the paper.

This work was supported in part by National Institutes of Health Grant NS108695 and Pittsburgh Institute of Brain Disorders & Recovery startup funds. J.C. is the Richard King Mellon Professor of Neurology at the University of Pittsburgh and a recipient of the Senior Research Career Scientist Award from the Department of Veterans Affairs. J.C. was also supported by Veterans Affairs Merit Review Grants BX003377 and BX005290. We thank Patricia Strickler for excellent administrative support.

*Y.Z. and C.M. contributed equally to this work.

The authors declare no competing financial interests.

Correspondence should be addressed to Yejie Shi at y.shi@pitt.edu or Jun Chen at chenj2@upmc.edu.

<https://doi.org/10.1523/JNEUROSCI.0682-22.2022>

Copyright © 2022 the authors

Introduction

Traumatic brain injury (TBI) is a global health burden, and there is an unmet need for therapies that can stop progressive brain damage and promote functional restoration after TBI. Neuroinflammation is a key mechanism underlying secondary injury after TBI, whereby excessive inflammation sustains brain damage and hinders tissue repair (Kumar and Loane, 2012). The innate immune cells in the post-TBI brain, that is, resident microglia (Mi) and monocyte-derived macrophages (MΦ) that invade the brain through the disrupted blood–brain barrier, are major contributors to these inflammatory responses (Barrett et al., 2020; Witcher et al., 2021). Mi/MΦ

in the post-TBI brain are phenotypically heterogeneous and have dualistic impact on TBI outcomes depending on their proinflammatory or pro-repair phenotype (G. Wang et al., 2015; Kumar et al., 2016), yet no therapy has been developed to leverage the high degree of functional plasticity of these cells to treat TBI. Molecules that can control the interconversion between proinflammatory and pro-repair Mi/M Φ phenotypes therefore hold great promise for becoming therapeutic targets of TBI to facilitate the resolution of inflammation and recovery of neurologic functions.

One such molecular switch that can potentially modulate the phenotype of post-TBI Mi/M Φ is signal transducer and activator of transcription 1 (STAT1). A member of the STAT family of transcription factors, STAT1 can be activated by JAK kinases in canonical interferon signaling and bind to specific DNA sequence motifs to control gene expression (Ivashkiv and Donlin, 2014). The ability of STAT1 to directly induce the expression of proinflammatory factors, such as inducible nitric oxide synthase (iNOS) and interleukin (IL)-12 (Ivashkiv and Donlin, 2014), makes it a potent regulator of immune cell phenotype. Indeed, STAT1 is widely accepted to be an essential mediator of proinflammatory “M1” polarization in peripheral macrophages (Lawrence and Natoli, 2011). To date, whether STAT1 regulates the functional phenotype of brain Mi/M Φ and subsequently affects the outcome after TBI is unknown. Multiple previous studies have reported the activation of STAT1 in the brain after TBI (Sen et al., 2020; H. Wu et al., 2021). It is intriguing, however, that the postulated role of STAT1 in the post-injury brain is controversial. Some studies associated STAT1 activation with harmful injury responses in the brain, such as endoplasmic reticulum stress and cell death after TBI (Gao et al., 2020; Sen et al., 2020), whereas others reported elevation of STAT1 accompanying improved outcomes and even enhanced “M2” responses after TBI (H. Wu et al., 2021) or spinal cord injury (Chen et al., 2018). Not only is direct evidence on a role of STAT1 in TBI lacking, but it is also poorly understood which cell type(s) are responsible for the impact of STAT1 on TBI outcome. These critical knowledge gaps impede the development of STAT1 as a therapeutic target to treat TBI.

We hypothesized that STAT1 drives proinflammatory Mi/M Φ responses that aggravate brain injury and functional deficits after TBI. Combining cell type-specific profiling of STAT1 expression with *in vivo* conditional STAT1 KO approaches, we aimed to explore the causal links between STAT1 and Mi/M Φ functions after TBI. Furthermore, we tested the therapeutic effect of fludarabine, a selective STAT1 inhibitor, against TBI-induced neuroinflammation, brain injury, and long-term functional deficits in a mouse model.

Materials and Methods

Animals

C57BL/6J (RRID:IMSR_JAX:000664), *Stat1*^{−/−} (STAT1 KO; RRID:IMSR_JAX:012606), *STAT1*^{LoxP} (RRID:MMRRC_032054-JAX), and *Cx3cr1*^{CreER} (RRID:IMSR_JAX:021160) mice were purchased from The Jackson Laboratory. Microglia/macrophage-specific STAT1 KO (STAT1 mKO) mice were obtained by crossing the *Cx3cr1*^{CreER} mice (Parkhurst et al., 2013) and *STAT1*^{LoxP} mice (Klover et al., 2010) for two generations. The STAT1 mKO mice (genotype: *Cx3cr1*^{CreER/wt}; *Stat1*^{flox/flox}) were viable, fertile, and did not exhibit any gross physical or behavioral abnormalities. To induce gene deletion, STAT1 mKO mice received intraperitoneal injections of tamoxifen (Sigma-Aldrich T5648; 75 mg/kg daily for 4 d). Hemizygous *Cx3cr1*^{CreER} mice (genotype: *Cx3cr1*^{CreER/wt}; *Stat1*^{wt/wt}) served as age- and sex-matched WT control mice for the STAT1 mKO

mice and received the same tamoxifen treatments. Mice were subjected to experimental TBI 10 d after tamoxifen treatments.

Mice were housed in a specific pathogen-free facility with a 12 h light/dark cycle. Food and water were available *ad libitum*. All animal experiments were performed in accordance with the National Institutes of Health's *Guide for the care and use of laboratory animals*, approved by the University of Pittsburgh Institutional Animal Care and Use Committee, and reported in accordance with the ARRIVE guidelines (Kilkenny et al., 2010). Adult male mice at 12–16 weeks of age were used for *in vivo* studies, and neonatal mice of both sexes were used for *in vitro* cultures. Experimental group assignments were randomized with a lottery-drawing box, and surgeries and all outcome assessments were performed by investigators blinded to mouse genotype and experimental group assignment whenever possible.

Traumatic brain injury model

TBI was induced by unilateral controlled cortical impact (CCI), as previously described (Pu et al., 2021b). Briefly, mice were anesthetized with 5% isoflurane in a 67% N₂O/30% O₂ mixture through an induction chamber, and anesthesia was maintained during surgery with 1.5% isoflurane delivered through a nose cone. Mouse heads were stabilized in a stereotaxic frame, and a skin incision was made under aseptic conditions to expose the skull and bregma. A right parietal craniotomy (centered 0.5 mm anterior and 2.0 mm lateral to bregma; diameter: 3.5 mm) was prepared with a drill to expose the dura and cerebral cortex. CCI was performed with a pneumatically driven CCI device (Precision Systems and Instrumentation) using a 3 mm (diameter) flat-tipped impactor to compress the exposed brain tissue to a depth of 1.5 mm for dwell time of 150 ms at a peak velocity of 3.5 m/s. Rectal temperature was monitored and maintained at 37 ± 0.5°C with a heating pad during surgery. After surgery, the skin incision was closed, and mice were placed in a clean cage. Mice received subcutaneous injections of ketoprofen (2 mg/kg daily) as an analgesic for 3 d after CCI. Animals in sham groups were subjected to anesthesia, skin incision, and recovery but were not subjected to craniotomy preparation or CCI.

Pharmacological inhibition of STAT1

The STAT1 inhibitor fludarabine (Selleck Chemicals S1491) was dissolved in a vehicle consisting of 5% DMSO, 40% PEG300, 5% Tween 80, and 50% ddH₂O for *in vivo* use. Mice received intraperitoneal injections of fludarabine at 2, 5, or 10 mg/kg (in 120 μ l of vehicle solution) starting from 2 h after CCI and then daily for 5 d after CCI. To inhibit STAT1 *in vitro*, fludarabine was first dissolved in DMSO at 200 mM, followed by dilution in culture medium to obtain the desired concentration (25–200 μ M). An equal volume of DMSO was used as vehicle control.

Behavior tests

Adhesive removal test. The adhesive removal test was performed as previously described (R. Wang et al., 2020a) to assess forepaw sensitivity and motor impairments. Briefly, an adhesive tape (0.3 × 0.3 cm) was applied to the left forepaw to cover the glabrous region. The latency to touch the tape (time to touch) and completely remove the tape (time to remove) were recorded, with a maximum of 120 s. Mice were trained for 3 d before the CCI or sham surgeries. After surgery, this test was performed for up to 35 d. Three trials were performed on each testing day, and the average latencies were calculated.

Foot fault test. The foot fault test was performed as described previously (R. Wang et al., 2020a) to assess sensorimotor coordination. Mice were placed on an elevated grid surface with a grid opening of 2.25 cm² and videotaped for 2 min from below the grid. The videotapes were analyzed by a blinded investigator to count the number of total steps and the number of foot faults made by the left limbs (impaired side; contralateral to CCI lesion). Foot faults were determined when the mouse misplaced its left forepaw or hindpaw such that the paw fell through the grid, and were expressed as a percentage of total steps.

Morris water maze test. The Morris water maze was used to assess cognitive functions, as described previously (Y. Shi et al., 2016). Briefly, a square platform (11 × 11 cm) was submerged 1.5 cm under the water surface in the center of one quadrant of a circular pool (diameter:

109 cm; depth: 33 ± 0.5 cm). Prominent spatial cues were displayed around the room. Nontoxic, white tempera paint was added to the water, and the temperature of the pool was maintained at $20 \pm 1^\circ\text{C}$. The test was composed of a spatial acquisition phase to assess learning capacity and a spatial retention phase to assess memory function. For the former, the mouse was placed in the pool in one of the three quadrants without the platform and allowed to swim for 60 s to find the hidden platform. This test was performed 3 d before CCI to habituate the mice to swimming and from days 29–33 after CCI. The time spent finding the hidden platform was recorded as the latency to escape from the forced swimming task, and the mean latency of three trials was quantified as a measure of spatial learning. At the end of each trial, the mouse was placed on the platform for 30 s. Spatial memory was evaluated on day 34 after CCI by removing the hidden platform. Each mouse was placed in the pool for a single 60 s probe trial. The number of crossings the mouse made toward where the platform was previously located was recorded as spatial memory.

Immunohistochemistry and data analyses

Mice were deeply anesthetized and transcardially perfused with 0.9% NaCl, followed by 4% PFA in PBS. Brains were harvested and cryoprotected in 30% sucrose in PBS, and frozen serial coronal brain sections (25- μm -thick) were prepared on a sliding microtome (Microm HM 450, Thermo Fisher Scientific). Sections were blocked with 5% donkey serum in PBS for 1 h, followed by overnight incubation at 4°C with the following primary antibodies: rabbit anti-Iba1 (Wako 019-19741), rat anti-CD16/CD32 (BD 553142), goat anti-arginase 1 (Arg1; Santa Cruz Biotechnology sc-18351), rabbit anti-NeuN (Millipore Sigma ABN78), mouse anti-neurofilament 200 (NF200; Millipore Sigma MAB5262), rabbit anti- β -amyloid precursor protein (β -APP; Thermo Fisher Scientific 51-2700), mouse anti-Caspr (Millipore Sigma MABN69), and rabbit anti-Nav1.6 (Alomone Labs ASC-009). For immunostaining involving mouse primary antibodies, a *Mouse on Mouse Immunodetection Kit* (Vector Laboratories BMK-2202) was used following the manufacturer's instructions. After washing, sections were incubated for 1 h at 20°C with donkey secondary antibodies conjugated with DyLight 488 or Cy3 fluorophores (1:1000, Jackson ImmunoResearch Laboratories). Alternate sections from each experimental condition were incubated in all solutions, except the primary antibodies to assess nonspecific secondary antibody staining. Sections were then mounted and coverslipped with Fluoromount-G containing DAPI (Southern Biotechnology). Fluorescence images were captured with an EVOS M7000 Cell Imaging System (Thermo Fisher Scientific), or with an Olympus Fluoview FV1000 confocal microscope and FV10-ASW 2.0 software.

Quantitative analyses of immunofluorescence staining images were performed manually by blinded investigators using the National Institutes of Health's ImageJ software. Brain injury after TBI was measured on six equally spaced coronal brain sections encompassing the brain lesion immunostained for NeuN. Tissue loss was calculated as the volume of the NeuN-immunopositive contralateral hemisphere minus that of the ipsilesional hemisphere. Viable neurons were counted in the peri-lesion cortex (at bregma 0.14 mm) and hippocampus (at bregma -1.34 mm) based on NeuN immunostaining under higher magnification. Iba1-immunopositive Mi/M Φ were counted from $40\times$ microscopic fields ($317.4\ \mu\text{m} \times 317.4\ \mu\text{m}$) in the peri-lesion cortex and striatum from 2–4 brain sections per mouse. Quantitative analyses of the nodes of Ranvier (NORs) were performed in $60\times$ microscopic fields with $2.5\times$ digital magnification (final area $83.97\ \mu\text{m} \times 83.97\ \mu\text{m}$) in the corpus callosum (CC) from 2 brain sections per mouse. NORs were identified as the Nav1.6-immunopositive regions with Caspr immunostaining on both sides (see Fig. 7E). Four parameters of the NORs were determined: (1) the number of morphologically intact NORs which had paranodal Caspr expression on both sides; (2) NOR length, measured as the distance between a pair of Caspr-immunostained paranodes (paranodal gap); (3) paranode length, measured as the average length of all Caspr-immunopositive areas in the field; and (4) Nav1.6-immunopositive area, measured as the average area of Nav1.6 fluorescence signals in all paranodal gaps in the field. Axonal injury was assessed in the CC, external capsule (EC), and striatum in 2 or 3 brain sections double-immunostained for β -APP and NF200. A

threshold was set for each brain section to differentiate the target signal from background. To measure β -APP- and NF200-immunopositive areas, ROIs were drawn in $40\times$ confocal microscopic fields to outline the CC and EC (see Fig. 2G, dashed line). Pixels positive for β -APP and NF200 in each ROI were then quantified and expressed as percentage of the total area of that ROI. NF200⁺ area in the ipsilesional hemisphere was further normalized to that of the noninjured contralateral side for each brain section.

The image-processing software Imaris (Bitplane) was used to reconstruct three-dimensional images of Iba1, CD16/32, and Arg1 immunofluorescence as we previously described (Liu et al., 2021). A z stack of 5 images spanning $10\ \mu\text{m}$ was imported into Imaris, and the immunosignal of each channel was remodeled to 3D images by the *surface* operation. Smoothing was set at $0.6\ \mu\text{m}$ for all channels and images. A threshold was set to differentiate the target signal from background. Nonspecific signals were then removed, and the 3D-rendered images were constructed. All images were processed with the same adjustments.

Flow cytometry

Mice were deeply anesthetized and transcardially perfused with ice-cold HBSS, and the ipsilesional and noninjured contralateral cerebral hemispheres were harvested. Single-cell suspensions were prepared from the mouse brain using the Miltenyi Biotec *Neural Tissue Dissociation Kit* (130-093-231) and gentleMACS Octo Dissociator with Heaters according to the manufacturer's instructions and as we described previously (L. Shi et al., 2020; R. Wang et al., 2020b). Suspensions were passed through a $70\ \mu\text{m}$ cell strainer, and fractionated on a 30% and 70% Percoll gradient at $800 \times g$ for 30 min to remove myelin and cell debris. Mononuclear cells at the interface were collected and resuspended at 1×10^7 cells/ml. The cells were first stained with the *Zombie NIR Fixable Viability Dye* (BioLegend 423105) for 20 min at 4°C for assessment of viability. The cells were then stained with fluorophore-conjugated antibodies recognizing surface antigens. After washing, cells were fixed and permeabilized with an eBioscience *Foxp3/Transcription factor Staining Buffer Set* (Thermo Fisher Scientific 00-5523-00) or 4% formaldehyde followed by ice-cold methanol, and then incubated with antibodies recognizing intracellular antigens. The following primary antibodies were used for flow cytometry: anti-Stat1 PE (BD 558537), anti-Ly6G BUV395 (Clone 1A8; BD 563978), anti-CD11b BUV737 (BD 612800), anti-CD45 PerCP-Cyanine5.5 (eBioscience 45-0451-82), anti-O4 AlexaFluor-488 (R&D Systems FAB1326G), anti-GLAST (ACSA-1) APC (Miltenyi Biotec 130-123-555), anti-CD45 eFlour 450 (eBioscience 48-0451-82), anti-CD11b APC-eFlour 780 (eBioscience 47-0112-82), anti-CD19 BUV737 (BD 612781), anti-CD3 APC (eBioscience 17-0032-82), anti-CD11c PerCP-Cyanine5.5 (eBioscience 45-0114-82), anti-F4/80 FITC (eBioscience 11-4801-82), anti-Ly6C BV605 (BD 563011), anti-CD16/CD32 BUV737 (BD 612783), anti-CD206 BV605 (BioLegend 141721), anti-CD86 PE-Cyanine5 (BioLegend 105016), anti-IL-10 BV421 (BD 563276), anti-Arg1 PE (R&D Systems IC5868P), and anti-TNF- α APC (eBioscience 17-7321-82). Flow cytometry was performed using a BD LSRFortessa Cell Analyzer driven by the FACSDiva software or a Cytek Aurora spectral analyzer driven by the SpectroFlo software. Fluorescence compensation was performed using single-stained *OneComp eBeads* (Thermo Fisher Scientific 01-1111-42) according to the manufacturer's instructions.

Data were analyzed using the FlowJo software to quantify positively stained cells. Furthermore, individual immune cells (CD45⁺ gated) were plotted using *tSNE* function in FlowJo to map high-dimensional cytometry data onto two dimensions based on the *fast interpolation-based t-distributed stochastic neighbor embedding* (Fit-SNE) algorithm (Linderman et al., 2019). *t-SNE* plots were generated with 1000 iterations of 6000 cells randomly selected from each mouse. Major cell types were identified according to their expression of prototypic markers.

Proteomic array analysis

Mice were deeply anesthetized and transcardially perfused with 0.9% NaCl, and fresh brain tissues were harvested. Protein was extracted from the ipsilesional and contralateral cerebral cortex using Cell Lysis Buffer (Cell Signaling 9803) with protease and phosphatase inhibitor cocktail

(Thermo Fisher Scientific 78842). The concentration of protein was measured using the Bradford protein assay. The content of 40 inflammatory factors was measured using a RayBiotech *Mouse Inflammation Array* kit (AAM-INF-1) following the manufacturer's instructions. Briefly, 250 μ g of protein was loaded to the membrane for each sample. The membrane was incubated with Biotinylated Antibody Cocktail at 4°C overnight, followed by incubation with HRP-Streptavidin at 4°C overnight. The membrane was then incubated with Detection Buffer mixture and processed for chemiluminescence detection. The signal intensity for each antigen-specific antibody spot was measured using ImageJ, and background signal averaged from three blank spots was subtracted. The signal intensity for each inflammatory factor was then normalized to the average intensity of the three positive control spots on each membrane. The concentrations of various factors were expressed as fold changes relative to noninjured baseline controls.

Primary microglia culture

Mixed primary glial cultures were prepared from 1- to 4-d-old neonatal mice. Briefly, the cerebrum was harvested, and meninges were carefully removed under a dissecting microscope. Dissociated cells were filtered through a 40 μ m cell strainer, and resuspended in culture medium (DMEM/F-12 with GlutaMAX supplement, 10% heat-inactivated FBS, 100 U/ml penicillin, and 100 μ g/ml streptomycin). The cells were then seeded into poly-D-lysine-coated T-75 cell culture flasks (1–2 brains per flask), and maintained in a humidified incubator at 37°C with 5% CO₂ and 95% air. After 12–14 d of incubation, microglia were detached from the astroglial layer by shaking the flasks on an orbital shaker at 180 rpm for 1 h. The enriched microglia were seeded in 24-well cell culture plates at a density of 1×10^5 cells per well. Experiments were performed 1 d after seeding.

To investigate the role of STAT1 in microglial responses, LPS (100 ng/ml; Sigma-Aldrich L4391) and interferon γ (IFN γ ; 20 ng/ml; PeproTech 315-05) were added to culture medium to stimulate microglia. Some cells were treated with the STAT1 inhibitor fludarabine at a concentration of 25–200 μ M for 24 h before LPS+IFN γ stimulation. Cell viability was assessed using a *LIVE/DEAD Viability/Cytotoxicity Kit* (Thermo Fisher Scientific L3224) following the manufacturer's instructions and as described previously (Mao et al., 2019), and fluorescence images were taken using the EVOS M7000 Cell Imaging System. The content of the proinflammatory mediators nitric oxide (NO) and TNF- α was measured in culture medium 24 h after LPS+IFN γ stimulation using a *Griess Reagent Nitrite Measurement Kit* (Cell Signaling 13547) and a *Mouse TNF- α Quantikine ELISA Kit* (R&D Systems MTA00B), respectively, following the manufacturer's instructions.

Western blotting

Protein was extracted from cultured cells using RIPA lysis and extraction buffer (Cell Signaling 9806) with protease and phosphatase inhibitor cocktail (Thermo Fisher Scientific 78842). The concentration of protein was measured using the Bradford protein assay. Equal amounts of protein samples were loaded onto acrylamide gels and subjected to electrophoresis, followed by transfer to Millipore Immobilon-FL PVDF membranes. Membranes were incubated in LI-COR Intercept Blocking Buffer for 1 h, followed by incubation with the following primary antibodies overnight at 4°C: rabbit anti-phospho-Stat1 (Tyr701; D4A7; Cell Signaling 7649), rabbit anti-Stat1 (D1K9Y; Cell Signaling 14994), and mouse anti- β -actin (Sigma-Aldrich A5441). After washing with TBS with Tween 20 (TBST; 137 mM NaCl, 20 mM Tris, 0.1% Tween 20, pH 7.6), membranes were incubated with LI-COR IRDye fluorescent secondary antibodies for 1 h at 20°C. Visualization and imaging were processed using a LI-COR Odyssey CLx Infrared Imaging System and Image Studio software. Immunoreactivity was semiquantitatively measured using Image Studio and normalized to the internal loading control.

Experimental design and statistical analysis

Datasets are presented as mean \pm SD. Individual data points are plotted where applicable. Normality of data distribution was tested with the Shapiro–Wilk test. Statistical comparison between two groups

was accomplished by the Student's *t* test (parametric) or Mann–Whitney *U* test (nonparametric). Differences in means among multiple groups were analyzed by one- or two-way ANOVA followed by the Bonferroni/Dunn *post hoc* correction. Pearson product linear regression analysis was used to correlate immunohistochemical parameters with neurobehavioral functions in the same cohort of mice. A *p* value <0.05 was deemed statistically significant, and all testing was two-tailed. All statistics are reported in the figure legends.

Results

STAT1 is elevated in Mi/M Φ after TBI and worsens TBI outcome

TBI-induced STAT1 activation in the brain has consistently been reported in previous studies (Sen et al., 2020; H. Wu et al., 2021). However, no study has hitherto explored which types of cells are responsible for the elevation of STAT1 in the post-TBI brain. We first examined the expression profiles of STAT1 in mouse brains after unilateral CCI, a model of moderate to severe TBI. Flow cytometry was used to identify major cell types in the brain, such as Mi/M Φ , astrocytes, oligodendrocytes, and other CNS cells, and to quantify STAT1-expressing cells at the acute (2 h) and subacute (24 and 72 h) stages after TBI (Fig. 1A). TBI induced robust elevation of STAT1 in the brain compared with noninjured sham controls, reflected by an increase of STAT1-immunopositive cells at 24 and 72 h after TBI (Fig. 1B). A further breakdown of all STAT1⁺ cells revealed that Mi/M Φ were the major cell population responsible for such changes. The percentage of Mi/M Φ expressing STAT1 was significantly higher than sham controls starting at 2 h after TBI, and remained elevated at 72 h after TBI (Fig. 1B). In contrast, the percentage of astrocytes, oligodendrocytes, and other CNS cells expressing STAT1 was unchanged at 2–72 h after TBI (Fig. 1B). On the other hand, Mi/M Φ consisted of 55.0% of all STAT1⁺ cells in sham brains, which further increased to 78.5% at 72 h after TBI (Fig. 1C). These data suggested a potentially important role for STAT1 in determining Mi/M Φ function at the subacute stage after TBI.

To date, it remains poorly understood whether STAT1 is good or bad in determining TBI outcomes, because no study so far has directly targeted STAT1 after TBI using pharmacological or genetic tools. Therefore, we tested the effect of fludarabine, a brain-penetrant and selective inhibitor of STAT1 (Frank et al., 1999), in mice after CCI. Since STAT1 upregulation mainly occurred in Mi/M Φ at the subacute injury stage, we administered fludarabine via intraperitoneal injection starting at 2 h after TBI and then daily for 5 d. Three dosages of fludarabine (2, 5, and 10 mg/kg/d) were tested, and the animals' sensorimotor function was examined for 14 d after TBI using the adhesive removal test (Fig. 1D) and foot fault test (Fig. 1E), both of which reliably detected TBI-induced sensorimotor deficits. In the adhesive removal test, all three dosages of fludarabine markedly improved the animals' performance over the testing period of 14 d, although the data were not significantly different among groups on day 14 (Fig. 1D). In the foot fault test, 5 and 10 mg/kg of fludarabine elicited improvement, whereas mice treated with 2 mg/kg of fludarabine demonstrated comparable performance with vehicle-treated mice (Fig. 1E). On day 14, mice treated with 5 mg/kg fludarabine still had significantly less hindpaw foot faults than vehicle-treated mice, while mice treated with 10 mg/kg of fludarabine demonstrated a statistical trend (*p* = 0.07) toward reducing both forepaw and hindpaw foot faults (Fig. 1E). These data suggest a detrimental role of

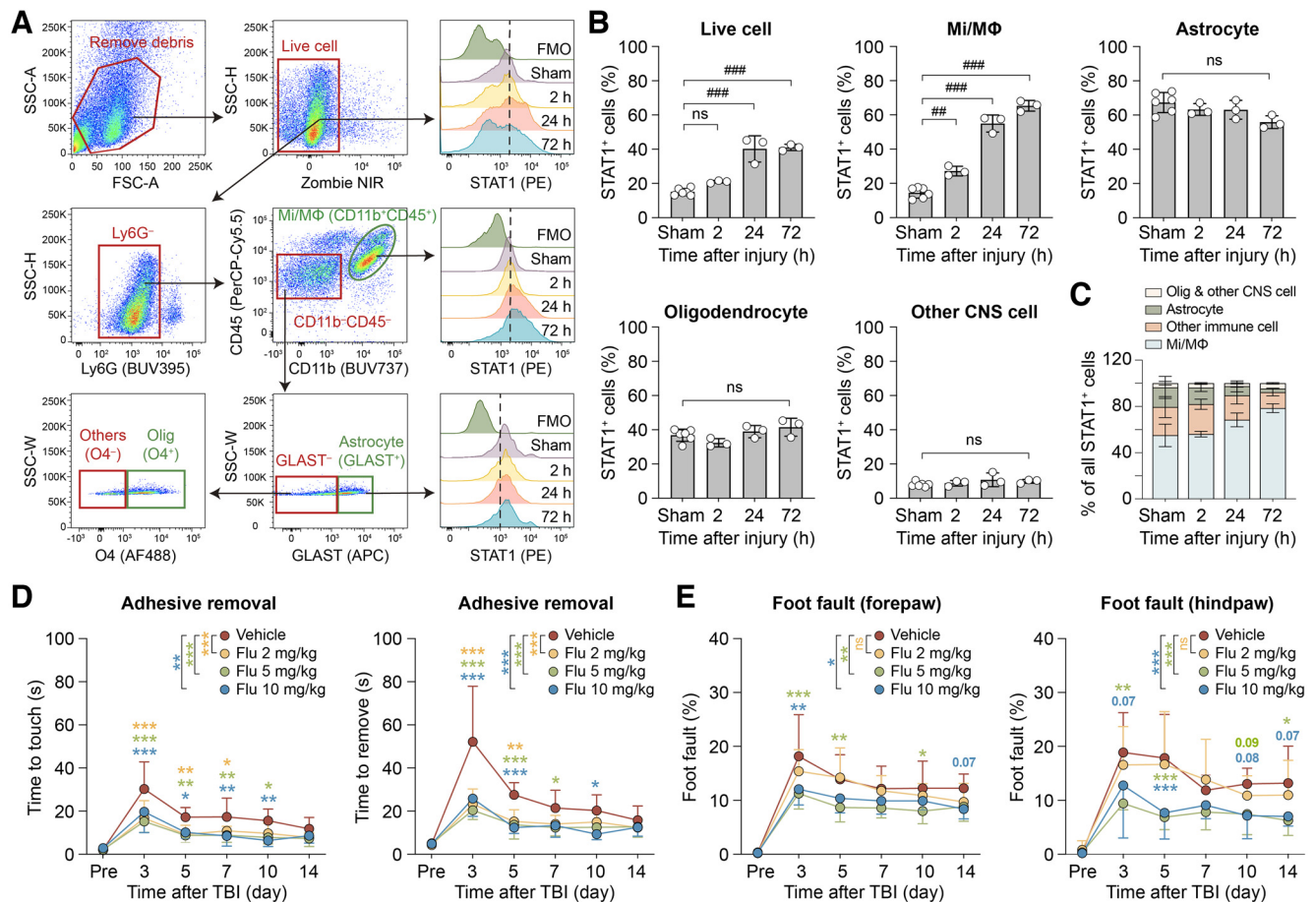


Figure 1. STAT1 is elevated in brain microglia/macrophages after TBI and worsens TBI outcome. **A–C**, Mice were subjected to TBI induced by CCI or sham injury. Expression of STAT1 in various types of cells in the brain was examined at 2, 24, and 72 h after TBI using flow cytometry. $n = 3$ –6 mice per group. **A**, Flow cytometry gating strategy for microglia/macrophages (Mi/MΦ; Ly6G⁺CD11b⁺CD45⁺), astrocytes (GLAST⁺), oligodendrocytes (Olig; O4⁺), and other CNS cells (CD11b⁺CD45⁻GLAST⁻O4⁻). STAT1-immunopositive cells were gated in each cell type based on the Fluorescence Minus One (FMO) control. **B**, The numbers of STAT1⁺ cells were quantified in all live cells, Mi/MΦ, astrocytes, oligodendrocytes, and other CNS cells, and were expressed as percentages of all cells of that type. One-way ANOVA and Bonferroni *post hoc*. Live cell: $F_{(3,11)} = 52.31$, $p < 0.0001$. 2 h versus sham $t_{(11)} = 2.306$, $p = 0.2496$; 24 h versus sham $t_{(11)} = 9.789$, $p < 0.0001$; 72 h versus sham $t_{(11)} = 10.10$, $p < 0.0001$. Mi/MΦ: $F_{(3,11)} = 182.7$, $p < 0.0001$. 2 h versus sham $t_{(11)} = 5.149$, $p = 0.0019$; 24 h versus sham $t_{(11)} = 16.42$, $p < 0.0001$; 72 h versus sham $t_{(11)} = 20.62$, $p < 0.0001$. Astrocyte: $F_{(3,11)} = 3.369$, $p = 0.0584$. Oligodendrocyte: $F_{(3,11)} = 3.116$, $p = 0.0704$. Other CNS cell: $F_{(3,11)} = 1.277$, $p = 0.3302$. **C**, Cellular composition of all STAT1⁺ live cells. More than 50% of STAT1⁺ cells were Mi/MΦ in all groups. **D**, **E**, Mice were subjected to TBI and received intraperitoneal injections of fludrabine (Flu) at 2, 5, or 10 mg/kg beginning at 2 h after TBI and then daily for 5 d. Neurologic deficits were assessed before (Pre) and up to 14 d after TBI using the adhesive removal (**D**) and foot fault (**E**) tests. $n = 7$ or 8 mice per group. Two-way repeated measures ANOVA and Bonferroni *post hoc*. **D**, Time to touch: $F_{(3,27)} = 9.854$, $p = 0.0001$. Main effect: 2 mg/kg versus vehicle $t_{(27)} = 4.191$, $p = 0.0008$; 5 mg/kg versus vehicle $t_{(27)} = 4.846$, $p = 0.0001$; 10 mg/kg versus vehicle $t_{(27)} = 4.058$, $p = 0.0011$. Individual day: 3 d-2 mg/kg versus vehicle $t_{(162)} = 5.199$, $p < 0.0001$; 5 mg/kg versus vehicle $t_{(162)} = 5.761$, $p < 0.0001$; 10 mg/kg versus vehicle $t_{(162)} = 3.920$, $p = 0.0004$. 5 d-2 mg/kg versus vehicle $t_{(162)} = 3.065$, $p = 0.0077$; 5 mg/kg versus vehicle $t_{(162)} = 3.274$, $p = 0.0039$; 10 mg/kg versus vehicle $t_{(162)} = 2.644$, $p = 0.0270$. 7 d-2 mg/kg versus vehicle $t_{(162)} = 2.503$, $p = 0.0399$; 5 mg/kg versus vehicle $t_{(162)} = 3.242$, $p = 0.0043$; 10 mg/kg versus vehicle $t_{(162)} = 3.296$, $p = 0.0036$. 10 d-2 mg/kg versus vehicle $t_{(162)} = 2.247$, $p = 0.0780$; 5 mg/kg versus vehicle $t_{(162)} = 2.953$, $p = 0.0109$; 10 mg/kg versus vehicle $t_{(162)} = 3.391$, $p = 0.0026$. Time to remove: $F_{(3,27)} = 16.14$, $p < 0.0001$. Main effect: 2 mg/kg versus vehicle $t_{(27)} = 5.283$, $p < 0.0001$; 5 mg/kg versus vehicle $t_{(27)} = 5.967$, $p < 0.0001$; 10 mg/kg versus vehicle $t_{(27)} = 5.616$, $p < 0.0001$. Individual day: 3 d-2 mg/kg versus vehicle $t_{(162)} = 7.979$, $p < 0.0001$; 5 mg/kg versus vehicle $t_{(162)} = 8.786$, $p < 0.0001$; 10 mg/kg versus vehicle $t_{(162)} = 7.023$, $p < 0.0001$. 5 d-2 mg/kg versus vehicle $t_{(162)} = 3.413$, $p = 0.0024$; 5 mg/kg versus vehicle $t_{(162)} = 3.851$, $p = 0.0005$; 10 mg/kg versus vehicle $t_{(162)} = 4.063$, $p = 0.0002$. 7 d-2 mg/kg versus vehicle $t_{(162)} = 2.052$, $p = 0.1252$; 5 mg/kg versus vehicle $t_{(162)} = 2.525$, $p = 0.0376$; 10 mg/kg versus vehicle $t_{(162)} = 2.171$, $p = 0.0943$. 10 d-2 mg/kg versus vehicle $t_{(162)} = 1.464$, $p = 0.4351$; 5 mg/kg versus vehicle $t_{(162)} = 2.133$, $p = 0.1033$; 10 mg/kg versus vehicle $t_{(162)} = 2.917$, $p = 0.0121$. **E**, Forepaw: $F_{(3,27)} = 4.742$, $p = 0.0088$. Main effect: 2 mg/kg versus vehicle $t_{(27)} = 1.017$, $p = 0.9544$; 5 mg/kg versus vehicle $t_{(27)} = 3.358$, $p = 0.0070$; 10 mg/kg versus vehicle $t_{(27)} = 2.702$, $p = 0.0353$. Individual day: 3 d-2 mg/kg versus vehicle $t_{(162)} = 1.647$, $p = 0.3048$; 5 mg/kg versus vehicle $t_{(162)} = 4.003$, $p = 0.0003$; 10 mg/kg versus vehicle $t_{(162)} = 3.649$, $p = 0.0011$. 5 d-2 mg/kg versus vehicle $t_{(162)} = 0.1783$, $p > 0.9999$; 5 mg/kg versus vehicle $t_{(162)} = 3.027$, $p = 0.0086$; 10 mg/kg versus vehicle $t_{(162)} = 2.128$, $p = 0.1046$. 10 d-2 mg/kg versus vehicle $t_{(162)} = 0.8142$, $p > 0.9999$; 5 mg/kg versus vehicle $t_{(162)} = 2.463$, $p = 0.0445$; 10 mg/kg versus vehicle $t_{(162)} = 1.408$, $p = 0.4833$. 14 d-2 mg/kg versus vehicle $t_{(162)} = 1.520$, $p = 0.3916$; 5 mg/kg versus vehicle $t_{(162)} = 1.986$, $p = 0.1463$; 10 mg/kg versus vehicle $t_{(162)} = 2.300$, $p = 0.0682$. Hindpaw: $F_{(3,27)} = 13.18$, $p < 0.0001$. Main effect: 2 mg/kg versus vehicle $t_{(27)} = 0.7755$, $p > 0.9999$; 5 mg/kg versus vehicle $t_{(27)} = 5.219$, $p < 0.0001$; 10 mg/kg versus vehicle $t_{(27)} = 4.249$, $p = 0.0007$. Individual day: 3 d-2 mg/kg versus vehicle $t_{(162)} = 0.8897$, $p > 0.9999$; 5 mg/kg versus vehicle $t_{(162)} = 3.664$, $p = 0.0010$; 10 mg/kg versus vehicle $t_{(162)} = 2.284$, $p = 0.0710$. 5 d-2 mg/kg versus vehicle $t_{(162)} = 0.4636$, $p > 0.9999$; 5 mg/kg versus vehicle $t_{(162)} = 4.274$, $p < 0.0001$; 10 mg/kg versus vehicle $t_{(162)} = 3.817$, $p = 0.0006$. 10 d-2 mg/kg versus vehicle $t_{(162)} = 0.8445$, $p > 0.9999$; 5 mg/kg versus vehicle $t_{(162)} = 2.171$, $p = 0.0941$; 10 mg/kg versus vehicle $t_{(162)} = 2.219$, $p = 0.0837$. 14 d-2 mg/kg versus vehicle $t_{(162)} = 0.8728$, $p > 0.9999$; 5 mg/kg versus vehicle $t_{(162)} = 2.699$, $p = 0.0231$; 10 mg/kg versus vehicle $t_{(162)} = 2.313$, $p = 0.0659$. Data are mean \pm SD. ** $p < 0.01$; *** $p < 0.001$; fludrabine versus vehicle control. * $p < 0.05$;

STAT1 in determining TBI outcome. In subsequent studies, we selected 5 mg/kg as the dosage of fludarabine and further investigated the mechanisms underlying its therapeutic effect against TBI.

Inhibition of STAT1 mitigates brain inflammation and subacute brain injury after TBI

TBI rapidly triggers activation of microglia and invasion of blood-borne immune cells into the brain, propelling a cascade of inflammatory responses. As expected, we detected remarkable infiltration of peripheral immune cells, such as T cells, B cells, neutrophils, dendritic cells, and M Φ in the ipsilesional brain hemisphere 5 d after TBI using flow cytometry (Fig. 2A). The number of microglia (CD11b⁺CD45^{low} cells) was smaller in the ipsilesional brain hemisphere than in the noninjured contralateral side (Fig. 2B), possibly because of some microglia upregulating CD45 during activation and becoming indistinguishable from the macrophage population (CD11b⁺CD45^{high} cells). The dramatic increase of peripheral immune cells after TBI could also reduce the relative portion of microglia per 10³ total cells (Fig. 2B). Post-TBI fludarabine treatment for 5 d (5 mg/kg intraperitoneally) significantly reduced the number of T cells, neutrophils, and M Φ in the brain (Fig. 2B), suggesting that fludarabine alleviates neuroinflammation burden. Interestingly, only Ly6C-expressing proinflammatory M Φ were reduced by fludarabine, whereas their Ly6C-negative patrolling and reparative counterparts (Geissmann et al., 2010) were unchanged (Fig. 2B). Such an anti-inflammatory effect of fludarabine was further confirmed by proteomic array screening of 40 inflammatory cytokines in the brain 5 d after TBI (Fig. 2C). Of the 40 inflammation markers measured, 14 were upregulated after TBI compared with the noninjured baseline controls, such as IL-1 β , TIMP-1, and IFN γ (Fig. 2D). Fludarabine treatment significantly reduced the levels of nine cytokines, including IL-1 β , IL-17A, and TNFR1 (Fig. 2D). We further assessed the phenotype of Mi/M Φ 5 d after TBI using double-label immunofluorescence staining of Iba1 with a proinflammatory marker CD16/32 or a pro-repair marker Arg1 (Hu et al., 2015). We focused on the peri-lesion cortex and striatum, both of which are vulnerable to TBI-induced damage and harbor overt activation of Iba1⁺ Mi/M Φ at the subacute injury stage (G. Wang et al., 2013). Compared with the noninjured contralateral brain where most Iba1⁺ cells were quiescent with no detectable CD16/32 or Arg1 immunosignal, the ipsilesional brain had markedly more Iba1⁺CD16/32⁺ cells and Iba1⁺Arg1⁺ cells (Fig. 2E). There were significantly less CD16/32⁺ proinflammatory Mi/M Φ in the cortex of fludarabine-treated mice compared with vehicle controls, and a concomitant increase of Arg1⁺ pro-repair Mi/M Φ in both the cortex ($p=0.0545$) and striatum ($p<0.05$) of fludarabine-treated mice (Fig. 2E). Together, these data suggest that the STAT1 inhibitor fludarabine effectively mitigates brain inflammation after TBI and particularly, exerts phenotype-modulating effects on Mi/M Φ by shifting their overall phenotype to favor the resolution of neuroinflammation.

Next, we examined whether fludarabine-induced changes in Mi/M Φ phenotype and brain inflammation milieu were associated with less tissue injury after TBI. We measured the gross tissue loss on serial coronal brain sections encompassing the lesion immunostained for the neuronal marker NeuN 5 d after TBI, which showed significantly smaller tissue loss volume in fludarabine-treated mice than vehicle controls (Fig. 2F). In parallel, we assessed axonal injury 5 d after TBI using double-label immunofluorescence staining of the axonal marker NF200 and β -APP, a marker for axonal injury (Fig. 2G) (Xia et al., 2018). TBI-induced

β -APP accumulation in the ipsilesional CC was significantly reduced in fludarabine-treated mice than vehicle controls (Fig. 2G). Striatal area immunopositive for NF200 was also larger in fludarabine-treated mice (Fig. 2G), suggesting improved axonal integrity. These data suggest that the anti-inflammatory and pro-repair Mi/M Φ phenotype cultivated by STAT1 inhibition was accompanied by less brain injury at the subacute stage after TBI.

STAT1 deficiency ameliorates proinflammatory microglial responses *in vitro*

Our data obtained from the *in vivo* CCI model strongly suggest that inhibition of STAT1 using fludarabine changes Mi/M Φ functional phenotype. Since fludarabine could target all types of cells after systemic administration *in vivo*, we examined its direct effect on microglia using *in vitro* cultures. Primary mouse microglia were treated with the canonical proinflammatory stimuli LPS plus IFN γ to mimic the proinflammatory environment in the post-TBI brain. LPS+IFN γ stimulation induced strong phosphorylation of STAT1 in microglia, starting from 2 h and lasting for 24 h after stimulation (Fig. 3A). LPS+IFN γ also upregulated expression of STAT1 protein at 6–24 h. As expected, microglia acquired a proinflammatory phenotype after LPS+IFN γ treatment, manifested by robust production of NO (Fig. 3B). Importantly, fludarabine reduced NO production from microglia 24 h after LPS+IFN γ stimulation in a dose-dependent manner, wherein 200 μ M of fludarabine demonstrated the most efficacy (Fig. 3B). Neither LPS+IFN γ stimuli nor fludarabine treatment induced cell death (Fig. 3C), suggesting functional modulation on microglia instead of changes in cell viability. Consistent with a previous report that fludarabine depletes STAT1 mRNA and protein (Frank et al., 1999), STAT1 phosphorylation and expression were largely abolished after 24 h of fludarabine treatment (Fig. 3D). Microglial production of another proinflammatory cytokine TNF- α was also significantly reduced by 200 μ M of fludarabine treatment (Fig. 3E).

To further confirm that fludarabine achieved these anti-inflammatory effects through inhibiting STAT1, rather than off-target effects, we examined the phenotype of STAT1-null microglia cultured from global STAT1 KO mice. We found that STAT1 KO largely reproduced the effect of fludarabine on inhibiting microglial production of NO (Fig. 3F) and TNF- α (Fig. 3G). Interestingly, while loss of STAT1 reduced microglial production of TNF- α by 63% (Fig. 3G), LPS+IFN γ -induced production of NO was almost completely blocked in STAT1 KO microglia (Fig. 3F), suggesting near-total dependence of the NO synthesis pathway on STAT1. These results were consistent with previous report (Stempel et al., 2007) that epithelial cells lacking STAT1 could not express iNOS on LPS+IFN γ stimulation, leading to subsequent deficiency to synthesize NO. More importantly, fludarabine did not further reduce NO and TNF- α production from STAT1 KO cells (Fig. 3F,G), indicating that STAT1 is essential for fludarabine's phenotype-modulating effect on microglia. Together, these proof-of-concept *in vitro* studies suggest that both genetic deletion and pharmacological inhibition of STAT1 ameliorate proinflammatory responses of microglia.

In vivo selective KO of STAT1 in Mi/M Φ replicates the effect of fludarabine to inhibit proinflammatory and destructive Mi/M Φ responses after TBI

We further validated the causal relationship between STAT1 and proinflammatory Mi/M Φ responses after TBI using the *in vivo*

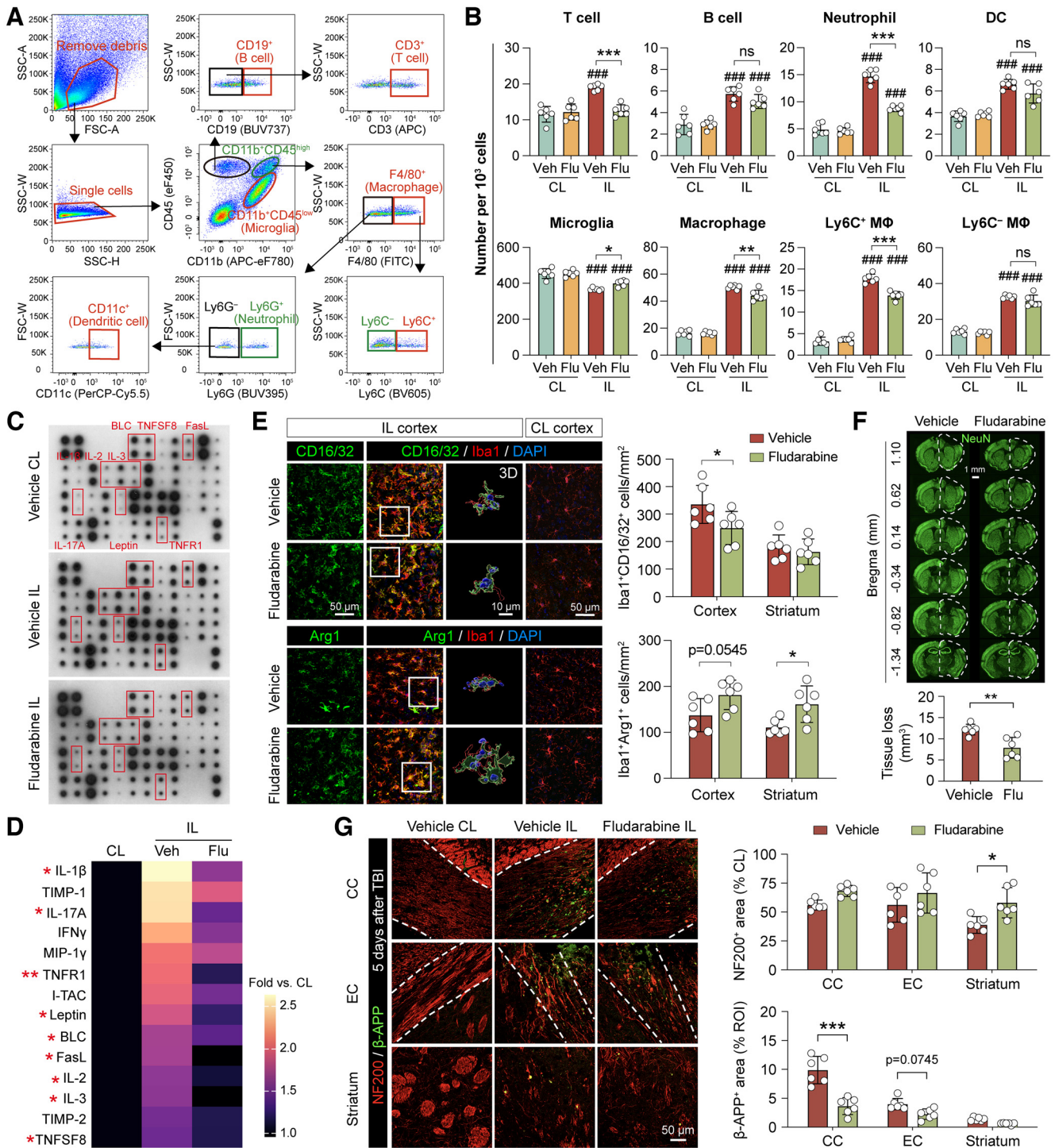


Figure 2. Inhibition of STAT1 with fludarabine mitigates neuroinflammation and subacute brain injury after TBI. Mice were subjected to TBI, and were treated with fludarabine (Flu; 5 mg/kg) or vehicle for 5 d. **A**, **B**, Infiltration of peripheral immune cells into the post-TBI brain was assessed using flow cytometry 5 d after TBI. $n = 6$ mice per group. **A**, Flow cytometry gating strategy for various immune cells in the brain. Macrophages (MΦ) were further gated into Ly6C⁺ and Ly6C⁻ subpopulations. **B**, The numbers of immune cells in the ipsilesional (IL) and noninjured contralesional (CL) brain hemispheres were quantified. One-way ANOVA and Bonferroni *post hoc*. T cell: $F_{(3,20)} = 22.06$, $p < 0.0001$. Veh IL versus CL $t_{(20)} = 7.121$, $p < 0.0001$; Flu IL versus CL $t_{(20)} = 0.3327$, $p > 0.9999$; IL Flu versus veh $t_{(20)} = 6.167$, $p < 0.0001$. B cell: $F_{(3,20)} = 26.97$, $p < 0.0001$. Veh IL versus CL $t_{(20)} = 7.119$, $p < 0.0001$; Flu IL versus CL $t_{(20)} = 5.349$, $p = 0.0002$; IL Flu versus veh $t_{(20)} = 1.786$, $p = 0.5354$. Neutrophil: $F_{(3,20)} = 167.9$, $p < 0.0001$. Veh IL versus CL $t_{(20)} = 19.12$, $p < 0.0001$; Flu IL versus CL $t_{(20)} = 8.027$, $p < 0.0001$; IL Flu versus veh $t_{(20)} = 11.61$, $p < 0.0001$. Dendritic cell: $F_{(3,20)} = 39.97$, $p < 0.0001$. Veh IL versus CL $t_{(20)} = 9.084$, $p < 0.0001$; Flu IL versus CL $t_{(20)} = 5.942$, $p < 0.0001$; IL Flu versus veh $t_{(20)} = 2.589$, $p = 0.1053$. Microglia: $F_{(3,20)} = 32.78$, $p < 0.0001$. Veh IL versus CL $t_{(20)} = 8.277$, $p < 0.0001$; Flu IL versus CL $t_{(20)} = 4.980$, $p = 0.0004$; IL Flu versus veh $t_{(20)} = 3.234$, $p = 0.0249$. Macrophage: $F_{(3,20)} = 337.0$, $p < 0.0001$. Veh IL versus CL $t_{(20)} = 24.36$, $p < 0.0001$; Flu IL versus CL $t_{(20)} = 20.16$, $p < 0.0001$; IL Flu versus veh $t_{(20)} = 4.461$, $p = 0.0014$. Ly6C⁺ macrophage: $F_{(3,20)} = 416.8$, $p < 0.0001$. Veh IL versus CL $t_{(20)} = 28.65$, $p < 0.0001$; Flu IL versus CL $t_{(20)} = 20.14$, $p < 0.0001$; IL Flu versus veh $t_{(20)} = 7.709$, $p < 0.0001$. Ly6C⁻ macrophage: $F_{(3,20)} = 189.8$, $p < 0.0001$. Veh IL versus CL $t_{(20)} = 17.49$, $p < 0.0001$; Flu IL versus CL $t_{(20)} = 16.11$, $p < 0.0001$; IL Flu versus veh $t_{(20)} = 2.068$, $p = 0.3112$. **C**, **D**, A panel of 40 inflammatory markers was measured in the IL brain hemisphere 5 d after TBI. Noninjured CL hemispheres were used as baseline control. $n = 5$ or 6 mice per group. **C**, Representative blots with significantly altered markers labeled. **D**, Heatmap represents the mean expression levels of 14 markers significantly upregulated in vehicle-treated TBI brains compared with baseline control. Control group was pooled from both vehicle- and fludarabine-treated mice, between which there were no differences. One-way ANOVA and Bonferroni *post hoc*. IL-1 β : $F_{(2,14)} = 10.62$, $p = 0.0016$; Veh IL versus

CCI model. To this end, we generated conditional STAT1 KO mice based on the Cre-lox system (Fig. 4A), which allowed us to delete STAT1 only in Cx3cr1^{CreER}-expressing cells (i.e., Mi/MΦ) on tamoxifen treatment. These Mi/MΦ-targeted STAT1 KO (STAT1 mKO) mice were subjected to CCI, and the functional phenotype of Mi/MΦ was examined 3 d later using flow cytometry. We first identified major types of immune cells in the post-TBI brain based on the expression of CD45, CD11b, and Ly6G (Fig. 4B,C), and then selected Mi (Ly6G[−]CD11b⁺CD45^{low}) and MΦ (Ly6G[−]CD11b⁺CD45^{high}) for subsequent expression profiling with a panel of well-established proinflammatory (CD16/32, TNF-α, CD86) and pro-repair (CD206, Arg1, IL-10) phenotypic markers for Mi/MΦ (Fig. 4D,E) (Hu et al., 2015). Similar to the effect caused by fludarabine (Fig. 2B), STAT1 mKO reduced the total number of MΦ in the post-TBI brain compared with WT control mice (Fig. 4D), suggesting less inflammatory burden. To compensate for such a reduction in total MΦ numbers, we quantified the number of cells positive for each marker both as the absolute cell number (Fig. 4F, top panels) and as a percentage of total Mi or MΦ (Fig. 4F, bottom panels). Both the numbers and percentages of CD16/32, TNF-α, and CD86-expressing proinflammatory Mi were reduced in STAT1 mKO mice, whereas Mi-expressing pro-repair markers CD206, Arg1, and IL-10 were not different between STAT1

CL $t_{(14)} = 4.568$, $p = 0.0013$; Flu IL versus CL $t_{(14)} = 1.645$, $p = 0.3665$; IL Flu versus veh $t_{(14)} = 2.999$, $p = 0.0287$. IL-17A: $F_{(2,14)} = 10.44$, $p = 0.0017$; Veh IL versus CL $t_{(14)} = 4.452$, $p = 0.0016$; Flu IL versus CL $t_{(14)} = 1.216$, $p = 0.7326$; IL Flu versus veh $t_{(14)} = 3.293$, $p = 0.0160$. TNF1: $F_{(2,14)} = 9.958$, $p = 0.0020$; Veh IL versus CL $t_{(14)} = 4.210$, $p = 0.0026$; Flu IL versus CL $t_{(14)} = 0.7050$, $p > 0.9999$; IL Flu versus veh $t_{(14)} = 3.538$, $p = 0.0098$. Leptin: $F_{(2,14)} = 8.834$, $p = 0.0033$; Veh IL versus CL $t_{(14)} = 4.077$, $p = 0.0034$; Flu IL versus CL $t_{(14)} = 1.045$, $p = 0.9413$; IL Flu versus veh $t_{(14)} = 3.081$, $p = 0.0244$. BLC: $F_{(2,14)} = 26.64$, $p < 0.0001$; Veh IL versus CL $t_{(14)} = 7.268$, $p < 0.0001$; Flu IL versus CL $t_{(14)} = 4.068$, $p = 0.0035$; IL Flu versus veh $t_{(14)} = 3.389$, $p = 0.0132$. IL-2: $F_{(2,14)} = 6.366$, $p = 0.0108$; Veh IL versus CL $t_{(14)} = 3.374$, $p = 0.0136$; Flu IL versus CL $t_{(14)} = 0.5886$, $p > 0.9999$; IL Flu versus veh $t_{(14)} = 2.813$, $p = 0.0415$. IL-3: $F_{(2,14)} = 7.419$, $p = 0.0064$; Veh IL versus CL $t_{(14)} = 3.264$, $p = 0.0170$; Flu IL versus CL $t_{(14)} = 0.2424$, $p > 0.9999$; IL Flu versus veh $t_{(14)} = 3.495$, $p = 0.0107$. TNF5F8: $F_{(2,14)} = 8.465$, $p = 0.0039$; Veh IL versus CL $t_{(14)} = 4.071$, $p = 0.0034$; Flu IL versus CL $t_{(14)} = 1.418$, $p = 0.5342$; IL Flu versus veh $t_{(14)} = 2.719$, $p = 0.0498$. One-way ANOVA on ranks and Dunn's *post hoc*: FasL: $H_{(2)} = 8.724$, $p = 0.0061$; Veh IL versus CL $Z = 2.540$, $p = 0.0333$; Flu IL versus CL $Z = 0.1143$, $p > 0.9999$; IL Flu versus veh $Z = 2.649$, $p = 0.0242$. E, The phenotype of microglia/macrophages was examined in the IL cortex and striatum 5 d after TBI by CD16/32 and arginase 1 (Arg1) immunostaining, double-labeled with the microglial/macrophage marker Iba1. Left panels, Representative images taken from the IL cortex. Rectangle represents a cell enlarged and 3D-rendered in the third column. No double-positive cell was observed in the CL side. The numbers of Iba1⁺CD16/32⁺ cells and Iba1⁺Arg1⁺ cells were counted in the IL cortex and striatum and summarized in the right panels. $n = 6$ mice per group. Two-way ANOVA and Bonferroni *post hoc*. Iba1⁺CD16/32⁺ cells: $F_{(1,20)} = 4.895$, $p = 0.0387$. Fludarabine versus vehicle $t_{(20)} = 2.646$, $p = 0.0310$ (cortex); $t_{(20)} = 0.4833$, $p > 0.9999$ (striatum). Iba1⁺Arg1⁺ cells: $F_{(1,20)} = 12.91$, $p = 0.0018$. Fludarabine versus vehicle $t_{(20)} = 2.383$, $p = 0.0545$ (cortex); $t_{(20)} = 2.699$, $p = 0.0276$ (striatum). F, Tissue loss was assessed 5 d after TBI on serial coronal brain sections immunostained for the neuronal marker NeuN. Dashed line indicates the relative area of the contralateral hemisphere to illustrate ipsilateral tissue loss. $n = 6$ mice per group. Unpaired *t* test: $t_{(10)} = 3.833$, $p = 0.0033$. G, Axonal injury was assessed 5 d after TBI using NF200 and β-APP double-label immunostaining. Shown are representative images taken from the CC, EC, and striatum in the IL and CL brain hemispheres. Dashed line indicates the boundary of CC/EC. Right panels, NF200- and β-APP-immunopositive areas were measured and summarized. $n = 6$ mice per group. Two-way ANOVA and Bonferroni *post hoc*. NF200⁺ area: $F_{(1,30)} = 13.27$, $p = 0.0010$. Fludarabine versus vehicle $t_{(30)} = 1.856$, $p = 0.2197$ (CC); $t_{(30)} = 1.546$, $p = 0.3979$ (EC); $t_{(30)} = 2.907$, $p = 0.0204$ (striatum). β-APP⁺ area: $F_{(1,30)} = 47.20$, $p < 0.0001$. Fludarabine versus vehicle $t_{(30)} = 8.501$, $p < 0.0001$ (CC); $t_{(30)} = 2.363$, $p = 0.0745$ (EC); $t_{(30)} = 1.036$, $p = 0.9251$ (striatum). Data are mean ± SD. ### $p < 0.001$; IL versus CL. * $p < 0.05$; ** $p < 0.01$; *** $p < 0.001$; fludarabine versus vehicle.

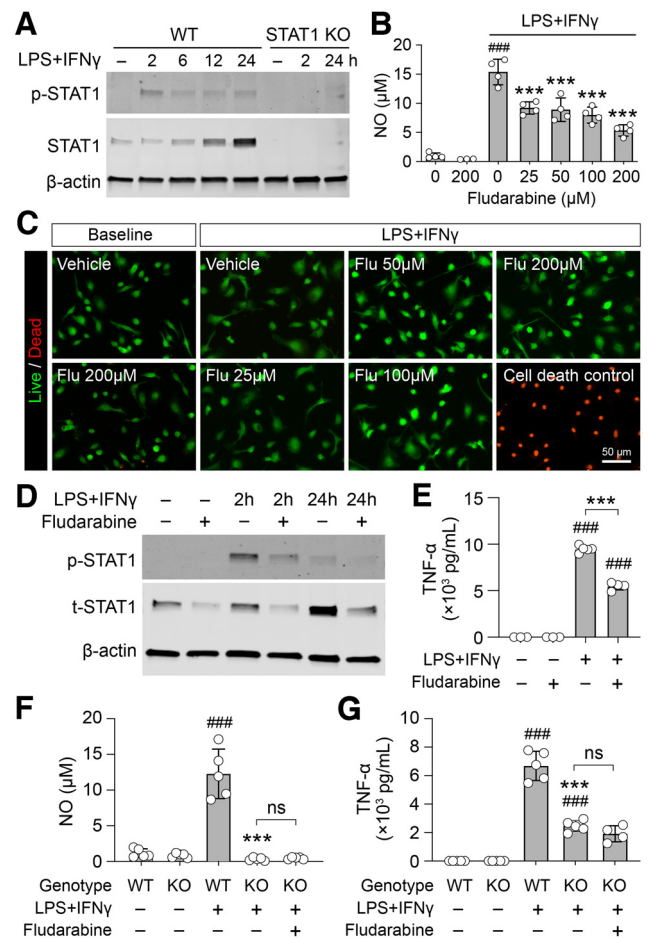


Figure 3. Inhibition or KO of STAT1 ameliorates proinflammatory microglial responses *in vitro*. Primary microglia were cultured from neonatal C57BL/6 (WT) mice or global STAT1 KO mice. Cells were treated with the STAT1 inhibitor fludarabine for 24 h, followed by stimulation with LPS (100 ng/ml) and IFN γ (20 ng/ml). **A**, Western blotting was performed at 2, 6, 12, and 24 h after LPS+IFN γ stimulation to assess phosphorylation of STAT1 (p-STAT1; Tyr701) and expression of total STAT1 in microglia. β -actin was used as an internal loading control. STAT1 KO microglia were used as negative control to demonstrate antibody specificity. **B**, **C**, Microglia were treated with 25, 50, 100, or 200 μ M of fludarabine. **B**, Microglial production of NO was measured in culture medium 24 h after LPS+IFN γ exposure. One-way ANOVA: $F_{(6,20)} = 51.23$, $p < 0.0001$. Bonferroni *post hoc*: LPS+IFN γ versus baseline $t_{(20)} = 14.53$, $p < 0.0001$; 25 μ M versus vehicle $t_{(20)} = 6.238$, $p < 0.0001$; 50 μ M versus vehicle $t_{(20)} = 6.542$, $p < 0.0001$; 100 μ M versus vehicle $t_{(20)} = 7.483$, $p < 0.0001$; 200 μ M versus vehicle $t_{(20)} = 10.14$, $p < 0.0001$. **C**, Cell viability was assessed 24 h after LPS+IFN γ stimulation using the live/dead assay. Cells treated with methanol served as positive control for cell death. **D–G**, Microglia were treated with 200 μ M of fludarabine or vehicle (DMSO) for 24 h, followed by LPS+IFN γ stimulation. **D**, Phospho-STAT1 and total STAT1 were measured by Western blotting at 2 and 24 h after LPS+IFN γ stimulation. **E**, The content of TNF- α in culture medium was measured by ELISA at 24 h after LPS+IFN γ exposure. One-way ANOVA: $F_{(3,11)} = 900.6$, $p < 0.0001$. Bonferroni *post hoc*: LPS+IFN γ + vehicle versus baseline + vehicle $t_{(11)} = 42.74$, $p < 0.0001$; LPS+IFN γ + fludarabine versus baseline + fludarabine $t_{(11)} = 23.66$, $p < 0.0001$; LPS+IFN γ + fludarabine versus LPS+IFN γ + vehicle $t_{(11)} = 19.60$, $p < 0.0001$. **F**, **G**, Production of NO (**F**) and TNF- α (**G**) from WT and STAT1 KO microglia 24 h after LPS+IFN γ stimulation, with or without fludarabine pretreatment. **F**, One-way ANOVA: $F_{(4,20)} = 53.58$, $p < 0.0001$. Bonferroni *post hoc*: WT LPS+IFN γ versus WT baseline $t_{(20)} = 11.07$, $p < 0.0001$; KO LPS+IFN γ versus KO baseline $t_{(20)} = 0.5159$, $p > 0.9999$; KO LPS+IFN γ versus WT LPS+IFN γ $t_{(20)} = 11.92$, $p < 0.0001$; KO LPS+IFN γ + fludarabine versus KO LPS+IFN γ $t_{(20)} = 0.1202$, $p > 0.9999$. **G**, One-way ANOVA: $F_{(4,19)} = 123.4$, $p < 0.0001$. Bonferroni *post hoc*: WT LPS+IFN γ versus WT baseline $t_{(19)} = 19.20$, $p < 0.0001$; KO LPS+IFN γ versus KO baseline $t_{(19)} = 7.052$, $p < 0.0001$; KO LPS+IFN γ versus WT LPS+IFN γ $t_{(19)} = 12.15$, $p < 0.0001$; KO LPS+IFN γ + fludarabine versus KO LPS+IFN γ $t_{(19)} = 1.475$, $p > 0.9999$. Data represent 3–5 independent cultures. Data are mean ± SD. ### $p < 0.001$; LPS+IFN γ versus baseline. *** $p < 0.001$; fludarabine versus vehicle control (**B**, **E**) or STAT1 KO versus WT (**F**, **G**).

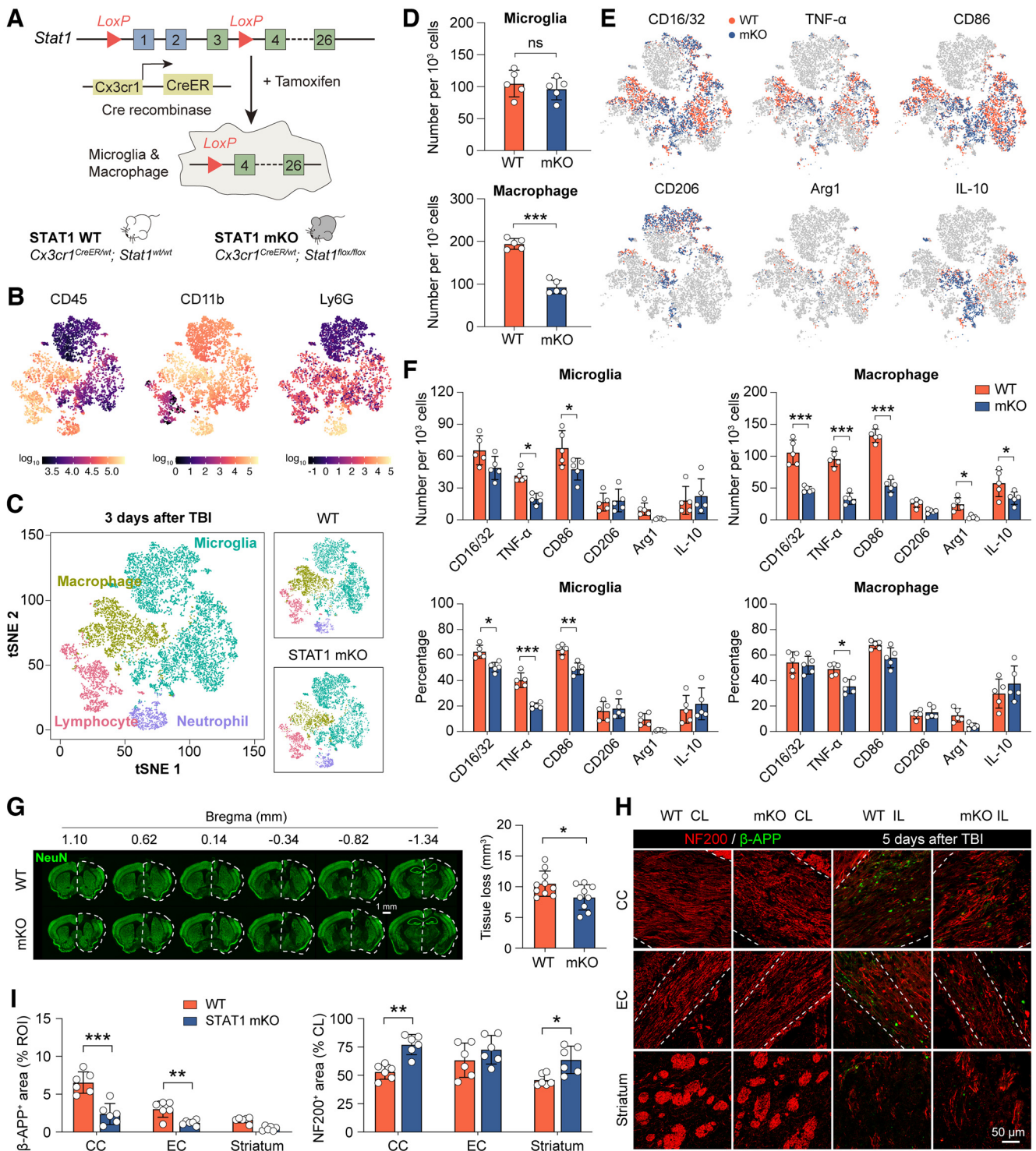


Figure 4. *In vivo* targeted KO of STAT1 alleviates proinflammatory responses of microglia and macrophages and subacute brain injury after TBI. **A**, Generation of microglia/macrophage-targeted STAT1 KO (*STAT1* mKO) mice. *LoxP* sites were engineered flanking the first two untranslated exons and the first translated exon of the *Stat1* gene. When crossed to *Cx3cr1^{CreER}* mice, the *LoxP* sites recombine and delete the floxed region of *Stat1*, knocking out the protein in CX3CR1-expressing cells in the presence of tamoxifen. **B–F**, *STAT1* mKO mice and WT control mice were subjected to TBI, and flow cytometry was performed 3 d after TBI to assess the phenotype of microglia and macrophages in the ipsilesional brain hemisphere. *n* = 5 mice per group. **B**, **C**, Representative t-SNE plots of 12,000 CD45⁺ cells pooled from one WT and one *STAT1* mKO mouse brain. Each dot represents one cell. Shown are the expression levels of prototypic cell markers in CD45⁺ cells (**B**) that identified major cell types in **C**: microglia (CD11b⁺CD45^{low}), macrophage (CD11b⁺CD45^{high}), neutrophil (Ly6G⁺), and lymphocyte (CD11b⁺CD45^{high}). Color represents fluorescence intensity on a logarithmic scale (**B**) or cell type (**C**). **D**, The numbers of microglia (Ly6G⁺CD11b⁺CD45^{low} cells) and macrophages (Ly6G⁺CD11b⁺CD45^{high} cells) were quantified. Unpaired *t* test: $t_{(8)} = 0.6955$, $p = 0.5064$ (microglia); $t_{(8)} = 11.13$, $p < 0.0001$ (macrophage). **E**, t-SNE plots of all microglia and macrophages illustrate cells from WT and *STAT1* mKO mice that were immunopositive for a panel of proinflammatory (CD16/32, TNF- α , CD86) and anti-inflammatory (CD206, arginase 1, IL-10) markers. **F**, The numbers of microglia and macrophages positive for each marker were determined after manual gating and expressed as cell number per 1000 single cells (top panels) or percentages of total microglia or macrophages (bottom panels). Two-way ANOVA and Bonferroni *post hoc*. Microglia number: $F_{(1,48)} = 13.78$, $p = 0.0005$. *STAT1* mKO versus WT $t_{(48)} = 2.442$, $p = 0.1100$ (CD16/32); $t_{(48)} = 3.193$, $p = 0.0149$ (TNF- α); $t_{(48)} = 2.940$, $p = 0.0302$ (CD86); $t_{(48)} = 0.2207$, $p > 0.9999$ (CD206); $t_{(48)} = 1.336$, $p > 0.9999$ (Arg1); $t_{(48)} = 0.5980$, $p > 0.9999$ (IL-10). Macrophage number: $F_{(1,48)} = 214.2$, $p < 0.0001$. *STAT1* mKO versus WT $t_{(48)} = 8.159$, $p < 0.0001$ (CD16/32); $t_{(48)} = 8.789$, $p < 0.0001$ (TNF- α); $t_{(48)} = 11.02$, $p < 0.0001$ (CD86); $t_{(48)} = 1.702$, $p = 0.5714$ (CD206); $t_{(48)} = 2.886$, $p = 0.0350$.

mKO and WT mice (Fig. 4F, left panels). In the MΦ population, CD16/32, TNF- α , and CD86-expressing proinflammatory cells outnumbered pro-repair cells, and were vastly less in STAT1 mKO mice than in WT mice (Fig. 4F, top right). However, after normalizing to the total MΦ number for each genotype, only TNF- α -expressing MΦ remained significantly less in STAT1 mKO mice than WT controls (Fig. 4F, bottom right). The proportion of MΦ expressing pro-repair markers CD206, Arg1, and IL-10 was unchanged by STAT1 mKO (Fig. 4F, bottom right). In summary, STAT1 deficiency caused differential changes of Mi and MΦ after TBI, yet the net effect was anti-inflammatory for both cell types, while STAT1 mKO led to specific reduction of proinflammatory Mi without changing total Mi numbers, the anti-inflammatory effect STAT1 mKO exerted on MΦ was mainly a result of decreased total MΦ.

We further assessed whether STAT1 mKO, through ameliorating proinflammatory Mi/MΦ responses after TBI, would have similar impact with fludarabine on reducing subacute brain injury. We found that the gross tissue loss volume was smaller in STAT1 mKO mice than WT mice 5 d after TBI (Fig. 4G). Consistently, axonal injury in the white matter-enriched regions (e.g., CC, EC, and striatum) was also reduced by STAT1 mKO, as reflected by less accumulation of β -APP and/or better preserved NF200 expression in STAT1 mKO mice 5 d after TBI (Fig. 4H,I). Therefore, STAT1 mKO directly modulates the phenotype of post-TBI Mi/MΦ, which subsequently leads to reduced brain injury at the subacute stage by alleviating the destructive responses of proinflammatory Mi/MΦ.

Mi/MΦ-targeted KO of STAT1 is sufficient to improve long-term outcomes after TBI

How important is the phenotype of Mi/MΦ in dictating long-term TBI outcomes? To tackle this question, we assessed neurologic deficits and tissue injury in STAT1 mKO mice for 35 d after TBI. The adhesive removal test (Fig. 5A,B) and foot fault test (Fig. 5C,D) were performed again, which detected sustained sensorimotor deficits caused by the CCI injury. While STAT1 mKO mice demonstrated similar performance with WT mice after sham operation, post-TBI STAT1 mKO mice had markedly improved performance compared with WT mice in both tests for at least 35 d after TBI (Fig. 5A–D). We also used the Morris water maze to assess the animals' cognitive functions. Our CCI model induced deficits in spatial learning but not in spatial

memory, reflected by increased escape latency (Fig. 5E) but similar numbers of platform crossings (Fig. 5F) between TBI- and sham-operated mice. STAT1 mKO did not reduce TBI-induced spatial learning deficits compared with WT controls at 29–33 d after TBI (Fig. 5E). Brain injury was significantly reduced in STAT1 mKO mice 35 d after TBI, as measured on serial coronal brain sections immunostained for NeuN (Fig. 5G,H). In summary, by modulating the phenotype of Mi/MΦ, STAT1 mKO was sufficient to promote long-term recovery of sensorimotor functions and to reduce chronic tissue injury after TBI.

Fludarabine improves long-term outcomes after TBI via inhibiting Mi/MΦ STAT1

Given the effect of fludarabine on modulating Mi/MΦ phenotype, we next examined whether post-TBI treatment with fludarabine could also improve long-term functional recovery. Fludarabine (5 mg/kg) was administered intraperitoneally at 2 h after TBI or sham injury and then daily for 5 d. The same set of neurobehavioral tests were used again to assess the sensorimotor and cognitive functions in mice for 35 d after injury (Fig. 6). Treatment with fludarabine did not alter the animals' performance after sham injury in any of the behavioral tests performed (Fig. 6A–C); therefore, we combined all animals undergoing sham injury as one sham group. In post-TBI mice, fludarabine not only improved the sensorimotor functions in the adhesive removal (Fig. 6D) and foot fault (Fig. 6E) tests, but also ameliorated spatial learning deficits in the Morris water maze (Fig. 6F). To test whether fludarabine had potential off-target effects, we assessed the effect of fludarabine on STAT1 mKO mice (Fig. 5; mKO TBI+Flu group). We found that fludarabine did not alter the behavioral performance of STAT1 mKO mice in the adhesive removal, foot fault, or Morris water maze tests (Fig. 5A–F). These results demonstrated promising therapeutic effects of fludarabine against post-TBI functional deficits, and suggest that STAT1 in Mi/MΦ is indispensable for fludarabine to achieve such beneficial effects.

Post-TBI fludarabine treatment improves long-term integrity of the brain

Finally, we examined the histologic basis underlying functional improvement on fludarabine treatment after TBI. Brain lesion volume was significantly reduced by fludarabine, as assessed on NeuN-immunostained coronal brain sections 35 d after TBI (Fig. 7A). A further examination of NeuN immunostaining under higher magnification revealed TBI-induced loss of neurons in the peri-lesion cortex and CA3 region of the hippocampus (Fig. 7B). We did not find significant changes in NeuN⁺ surviving neurons in the peri-lesion cortex and hippocampus in fludarabine-treated mice compared with vehicle controls (Fig. 7C), suggesting that fludarabine may promote functional recovery after TBI via improving the integrity of other brain regions, such as the white matter. Therefore, we examined the integrity of the NORs in the peri-lesion CC 35 d after TBI. Disruption of the NORs and adjacent paranodal domains where myelin attaches to axons is an important feature of white matter injury after TBI (Marion et al., 2018). Disorganized NORs and detachment of myelin at the paranodes occur within 24 h after injury and can last for weeks (Reeves et al., 2010; Marion et al., 2018). We identified the NORs using double-label immunostaining of sodium channel Nav1.6 and contactin-associated protein (Caspr), two axonal membrane proteins at the nodes and paranodes, respectively (Marion et al., 2018; R. Wang et al., 2020b), and assessed

←

(Arg1); $t_{(48)} = 3.294$, $p = 0.0112$ (IL-10). Microglia percentage: $F_{(1,48)} = 23.51$, $p < 0.0001$. STAT1 mKO versus WT $t_{(48)} = 2.901$, $p = 0.0336$ (CD16/32); $t_{(48)} = 4.784$, $p = 0.0001$ (TNF- α); $t_{(48)} = 3.610$, $p = 0.0044$ (CD86); $t_{(48)} = 0.4432$, $p > 0.9999$ (CD206); $t_{(48)} = 2.060$, $p = 0.2689$ (Arg1); $t_{(48)} = 1.034$, $p > 0.9999$ (IL-10). Macrophage percentage: $F_{(1,48)} = 4.790$, $p = 0.0335$. STAT1 mKO versus WT $t_{(48)} = 0.4748$, $p > 0.9999$ (CD16/32); $t_{(48)} = 2.997$, $p = 0.0259$ (TNF- α); $t_{(48)} = 2.176$, $p = 0.2070$ (CD86); $t_{(48)} = 0.4075$, $p > 0.9999$ (CD206); $t_{(48)} = 1.839$, $p = 0.4323$ (Arg1); $t_{(48)} = 1.718$, $p = 0.5531$ (IL-10). **G**, Tissue loss was assessed 5 d after TBI on serial coronal brain sections immunostained for NeuN. $n = 9$ or 10 mice per group. Unpaired t test: $t_{(17)} = 2.366$, $p = 0.0301$. **H**, Axonal injury was assessed 5 d after TBI using NF200 and β -APP double-label immunostaining. Shown are representative images taken from CC, EC, and striatum in the IL and CL brain hemispheres. Dashed line indicates the boundary of CC/EC. **I**, Summarized data on NF200- and β -APP-immunopositive areas. $n = 6$ mice per group. Two-way ANOVA and Bonferroni *post hoc*. NF200⁺ area: $F_{(1,30)} = 23.19$, $p < 0.0001$. STAT1 mKO versus WT $t_{(30)} = 3.932$, $p = 0.0014$ (CC); $t_{(30)} = 1.518$, $p = 0.4184$ (EC); $t_{(30)} = 2.892$, $p = 0.0212$ (striatum). β -APP⁺ area: $F_{(1,30)} = 55.11$, $p < 0.0001$. STAT1 mKO versus WT $t_{(30)} = 7.541$, $p < 0.0001$ (CC); $t_{(30)} = 3.271$, $p = 0.0081$ (EC); $t_{(30)} = 2.046$, $p = 0.1487$ (striatum). Data are mean \pm SD. * $p < 0.05$; ** $p < 0.01$; *** $p < 0.001$; STAT1 mKO versus WT.

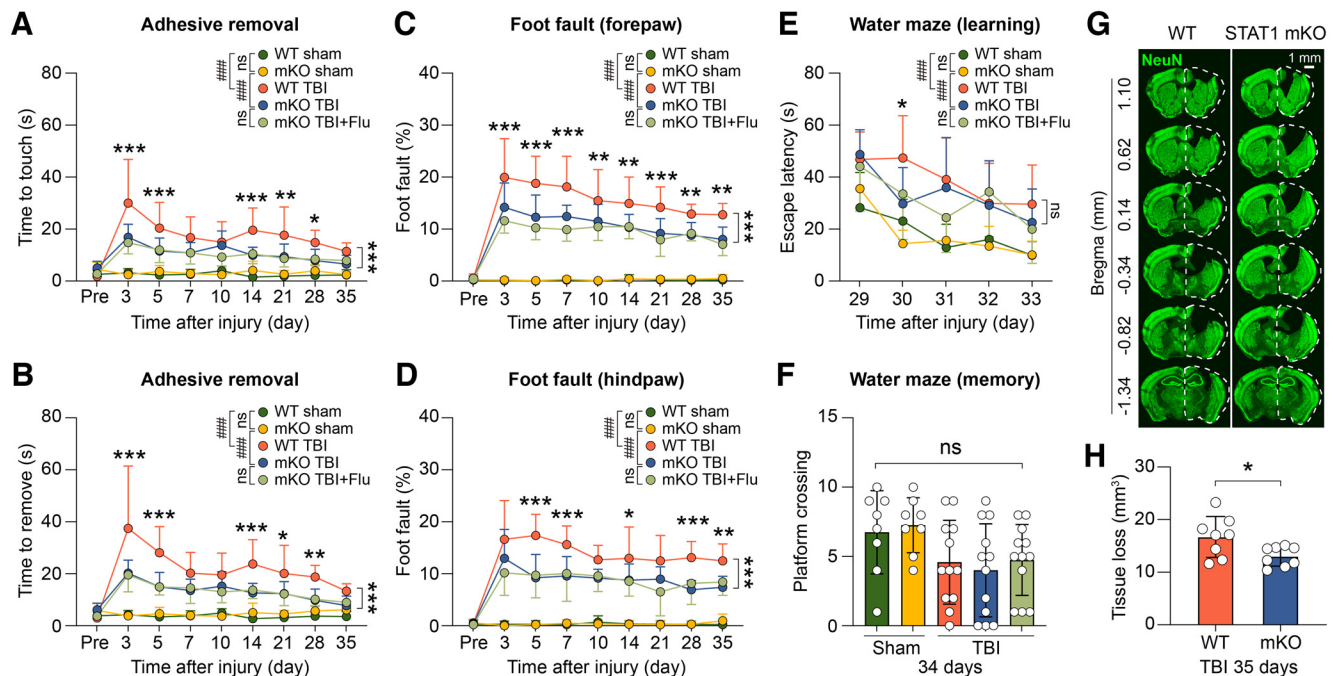


Figure 5. Selective deletion of STAT1 in microglia/macrophages is sufficient to improve long-term TBI outcomes. STAT1 mKO mice and WT mice were subjected to TBI induced by CCI or sham injury. One group of STAT1 mKO mice received post-TBI fludarabine treatment (Flu; 5 mg/kg) for 5 d. **A–D**, Sensorimotor deficits were assessed before (Pre) and up to 35 d after injury by the adhesive removal (**A,B**) and foot fault (**C,D**) tests. $n = 8$ (sham) or 12 (TBI) mice per group. Two-way repeated-measures ANOVA and Bonferroni *post hoc*. **A**, $F_{(4,47)} = 60.75$, $p < 0.0001$. Main effect: mKO sham versus WT sham $t_{(47)} = 0.5964$, $p > 0.9999$; WT TBI versus WT sham $t_{(47)} = 13.25$, $p < 0.0001$; mKO TBI versus mKO sham $t_{(47)} = 6.685$, $p < 0.0001$; mKO TBI versus WT TBI $t_{(47)} = 6.612$, $p < 0.0001$; mKO TBI+Flu versus mKO TBI $t_{(47)} = 0.8083$, $p > 0.9999$. mKO TBI versus WT TBI on individual day: $t_{(423)} = 6.158$, $p < 0.0001$ (day 3); $t_{(423)} = 4.127$, $p = 0.0004$ (day 5); $t_{(423)} = 4.505$, $p < 0.0001$ (day 14); $t_{(423)} = 3.867$, $p = 0.0013$ (day 21); $t_{(423)} = 3.242$, $p = 0.0128$ (day 28). **B**, $F_{(4,47)} = 55.15$, $p < 0.0001$. Main effect: mKO sham versus WT sham $t_{(47)} = 0.7811$, $p > 0.9999$; WT TBI versus WT sham $t_{(47)} = 12.77$, $p < 0.0001$; mKO TBI versus mKO sham $t_{(47)} = 5.838$, $p < 0.0001$; mKO TBI versus WT TBI $t_{(47)} = 6.798$, $p < 0.0001$; mKO TBI+Flu versus mKO TBI $t_{(47)} = 0.1444$, $p > 0.9999$. mKO TBI versus WT TBI on individual day: $t_{(423)} = 6.930$, $p < 0.0001$ (day 3); $t_{(423)} = 5.303$, $p < 0.0001$ (day 5); $t_{(423)} = 4.467$, $p = 0.0001$ (day 14); $t_{(423)} = 3.097$, $p = 0.0208$ (day 21); $t_{(423)} = 3.632$, $p = 0.0032$ (day 28). **C**, $F_{(4,47)} = 137.5$, $p < 0.0001$. Main effect: mKO sham versus WT sham $t_{(47)} = 0.1356$, $p > 0.9999$; WT TBI versus WT sham $t_{(47)} = 18.88$, $p < 0.0001$; mKO TBI versus mKO sham $t_{(47)} = 12.66$, $p < 0.0001$; mKO TBI versus WT TBI $t_{(47)} = 6.782$, $p < 0.0001$; mKO TBI+Flu versus mKO TBI $t_{(47)} = 1.633$, $p > 0.9999$. mKO TBI versus WT TBI on individual day: $t_{(423)} = 4.781$, $p < 0.0001$ (day 3); $t_{(423)} = 5.410$, $p < 0.0001$ (day 5); $t_{(423)} = 4.701$, $p < 0.0001$ (day 7); $t_{(423)} = 3.316$, $p = 0.0099$ (day 10); $t_{(423)} = 3.829$, $p = 0.0015$ (day 14); $t_{(423)} = 4.161$, $p = 0.0004$ (day 21); $t_{(423)} = 3.341$, $p = 0.0091$ (day 28); $t_{(423)} = 3.896$, $p = 0.0011$ (day 35). **D**, $F_{(4,47)} = 277.2$, $p < 0.0001$. Main effect: mKO sham versus WT sham $t_{(47)} = 0.07634$, $p > 0.9999$; WT TBI versus WT sham $t_{(47)} = 26.93$, $p < 0.0001$; mKO TBI versus mKO sham $t_{(47)} = 26.85$, $p < 0.0001$; mKO TBI versus WT TBI $t_{(47)} = 11.02$, $p < 0.0001$; mKO TBI+Flu versus mKO TBI $t_{(47)} = 0.4669$, $p > 0.9999$. mKO TBI versus WT TBI on individual day: $t_{(423)} = 6.178$, $p < 0.0001$ (day 5); $t_{(423)} = 4.581$, $p < 0.0001$ (day 7); $t_{(423)} = 3.212$, $p = 0.0142$ (day 14); $t_{(423)} = 4.726$, $p < 0.0001$ (day 28); $t_{(423)} = 3.894$, $p = 0.0011$ (day 35). **E, F**, The Morris water maze test was performed to assess spatial learning (**E**) and spatial memory (**F**) at 29–34 d after injury. $n = 8$ (sham) or 12 (TBI) mice per group. **E**, Two-way repeated-measures ANOVA and Bonferroni *post hoc*. $F_{(4,47)} = 13.88$, $p < 0.0001$. Main effect: mKO sham versus WT sham $t_{(47)} = 0.05537$, $p > 0.9999$; WT TBI versus WT sham $t_{(47)} = 5.803$, $p < 0.0001$; mKO TBI versus mKO sham $t_{(47)} = 4.359$, $p = 0.0007$; mKO TBI versus WT TBI $t_{(47)} = 1.683$, $p = 0.9907$; mKO TBI+Flu versus mKO TBI $t_{(47)} = 0.6104$, $p > 0.9999$. mKO TBI versus WT TBI on individual day: $t_{(423)} = 3.125$, $p = 0.0200$ (day 30). **F**, One-way ANOVA: $F_{(4,47)} = 2.333$, $p = 0.0694$. **G, H**, Chronic tissue loss was assessed 35 d after TBI on serial coronal brain sections immunostained for NeuN. $n = 8$ mice per group. **G**, Representative images showing NeuN immunofluorescence in 6 brain sections encompassing the TBI lesion. **H**, Summarized data on the volumes of brain tissue loss. Unpaired *t* test: $t_{(14)} = 2.425$, $p = 0.0294$. Data are mean \pm SD. ### $p < 0.001$; TBI versus sham. * $p < 0.05$; ** $p < 0.01$; *** $p < 0.001$; STAT1 mKO versus WT.

injury to the NORs in vehicle and fludarabine-treated mice 35 d after TBI (Fig. 7D). In vehicle-treated mice at 35 d after TBI, the ipsilesional CC had prominent disruption of the NOR structure, and the number of morphologically intact NORs, defined as the gap immunopositive for Nav1.6 between a pair of paranodal Caspr staining, was significantly less than the noninjured contralateral side (Fig. 7E). A closer examination on individual NOR revealed shorter length of paranodal Caspr immunosignal and a concomitant reduction of Nav1.6-immunopositive area at the nodes in the ipsilesional CC (Fig. 7E), both of which indicated TBI-induced NOR damage. The lengths of the NORs (paranodal gaps) were not different between TBI and sham groups. Importantly, fludarabine promoted long-term integrity of the peri-lesion white matter, whereby the number of normal NORs and the length of paranodes were significantly larger in fludarabine-treated mice than vehicle controls 35 d after TBI (Fig. 7E). Fludarabine treatment did not change the length of the NORs or the expression of Nav1.6 at the NORs (Fig. 7E).

Since our neurobehavioral tests and immunofluorescence staining at 35 d after TBI were performed on the same cohort of mice, we conducted linear regression analysis to explore the link underlying these parameters. The results showed that gross tissue loss volumes negatively correlated with the animals' performance in the adhesive removal test (Fig. 7F), and the numbers of intact NORs in the CC negatively correlated with the foot faults the animals made in the behavioral tests (Fig. 7G). In summary, fludarabine not only improves long-term sensorimotor and cognitive functions after TBI, but also ameliorates brain lesion and white matter injury, thereby presenting itself as a promising treatment to TBI.

Discussion

This study provided the first line of direct evidence on a destructive role of STAT1 after TBI, focusing on its phenotype-modulating effect on brain Mi/MΦ. Using Mi/MΦ-targeted conditional STAT1 mKO mice, we demonstrated a fundamental role of

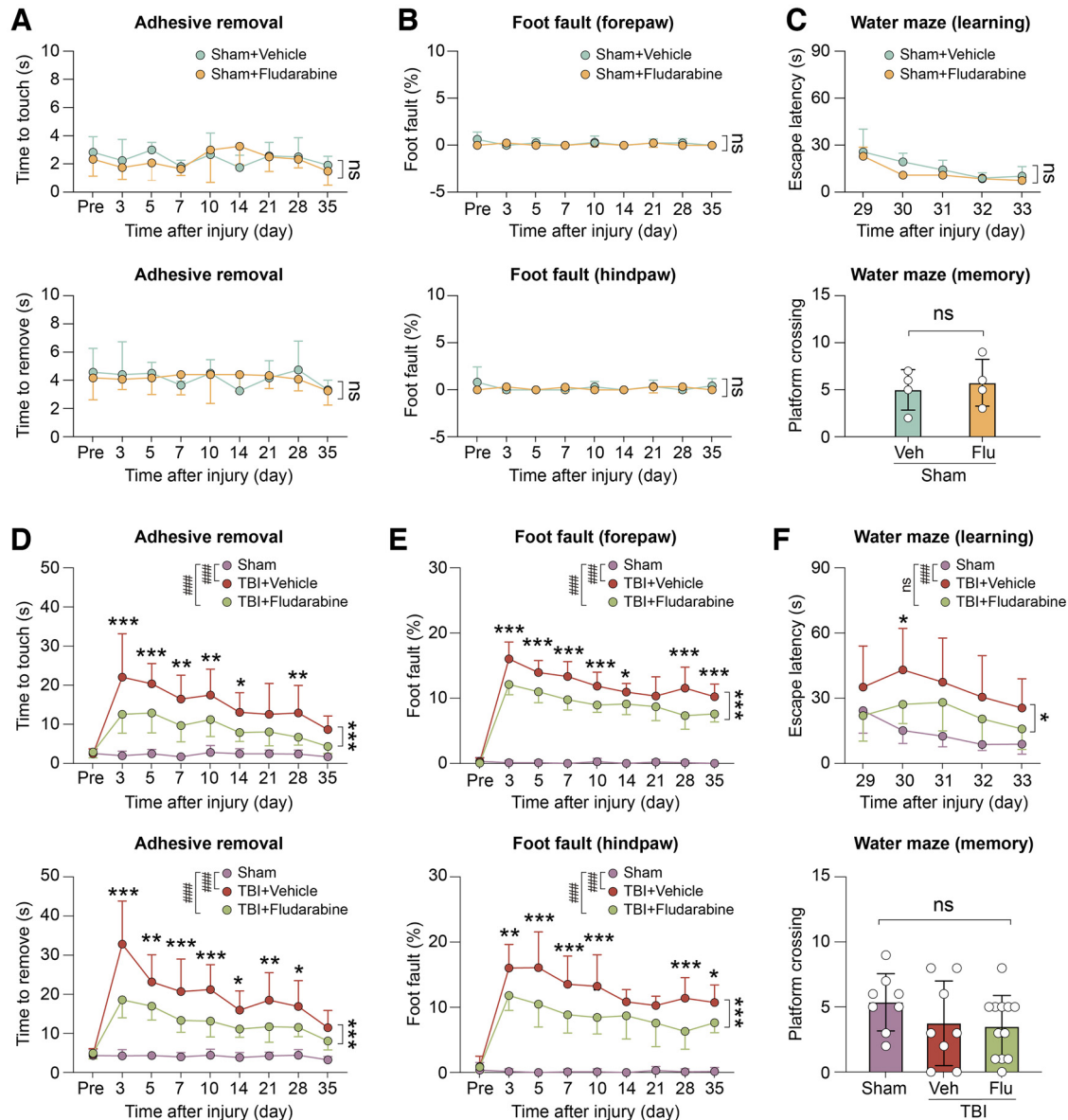


Figure 6. Post-TBI treatment with the STAT1 inhibitor fludarabine promotes long-term recovery of neurologic functions. Mice were subjected to TBI or sham injury, and were treated with fludarabine (5 mg/kg) or vehicle for 5 d. **A–C**, Sensorimotor deficits were assessed before (Pre) and up to 35 d after sham injury by the adhesive removal (**A**) and foot fault (**B**) tests. The Morris water maze test (**C**) was performed to assess spatial learning and spatial memory at 29–34 d after sham injury. Fludarabine- and vehicle-treated mice demonstrated similar performance in all tests after sham injury. $n = 4$ mice per group. Two-way repeated-measures ANOVA. **A**, Time to touch: $F_{(1,6)} = 0.02923$, $p = 0.8699$. Time to remove: $F_{(1,6)} = 0.001179$, $p = 0.9737$. **B**, Forepaw: $F_{(1,6)} = 3.419$, $p = 0.1139$. Hindpaw: $F_{(1,6)} = 0.3430$, $p = 0.5794$. **C**, Learning: $F_{(1,6)} = 3.653$, $p = 0.1045$. Unpaired t test: $t_{(6)} = 0.4540$, $p = 0.6658$ (**C**, memory). **D–F**, The adhesive removal test (**D**), foot fault test (**E**), and Morris water maze test (**F**) were performed to assess sensorimotor and cognitive functions for up to 35 d after TBI. Sham group was pooled from both vehicle- and fludarabine-treated mice, between which there were no differences. $n = 8$ –12 mice per group. Two-way repeated-measures ANOVA and Bonferroni *post hoc*. **D**, Time to touch: $F_{(2,25)} = 48.18$, $p < 0.0001$. Main effect: TBI+vehicle versus sham $t_{(25)} = 9.810$, $p < 0.0001$; TBI+fludarabine versus TBI+vehicle $t_{(25)} = 5.088$, $p < 0.0001$. TBI+fludarabine versus TBI+vehicle on individual day: $t_{(25)} = 4.965$, $p < 0.0001$ (day 3); $t_{(25)} = 3.934$, $p = 0.0003$ (day 5); $t_{(25)} = 3.571$, $p = 0.0013$ (day 7); $t_{(25)} = 3.288$, $p = 0.0035$ (day 10); $t_{(25)} = 2.686$, $p = 0.0233$ (day 14); $t_{(25)} = 3.230$, $p = 0.0043$ (day 28). Time to remove: $F_{(2,25)} = 82.76$, $p < 0.0001$. Main effect: TBI+vehicle versus sham $t_{(25)} = 12.82$, $p < 0.0001$; TBI+fludarabine versus TBI+vehicle $t_{(25)} = 6.121$, $p < 0.0001$. TBI+fludarabine versus TBI+vehicle on individual day: $t_{(25)} = 7.380$, $p < 0.0001$ (day 3); $t_{(25)} = 3.184$, $p = 0.0050$ (day 5); $t_{(25)} = 3.794$, $p = 0.0006$ (day 7); $t_{(25)} = 4.138$, $p = 0.0001$ (day 10); $t_{(25)} = 2.489$, $p = 0.0407$ (day 14); $t_{(25)} = 3.471$, $p = 0.0019$ (day 21); $t_{(25)} = 2.747$, $p = 0.0195$ (day 28). **E**, Forepaw: $F_{(2,25)} = 753.6$, $p < 0.0001$. Main effect: TBI+vehicle versus sham $t_{(25)} = 36.83$, $p < 0.0001$; TBI+fludarabine versus TBI+vehicle $t_{(25)} = 9.910$, $p < 0.0001$. TBI+fludarabine versus TBI+vehicle on individual day: $t_{(25)} = 5.414$, $p < 0.0001$ (day 3); $t_{(25)} = 4.093$, $p = 0.0002$ (day 5); $t_{(25)} = 4.937$, $p < 0.0001$ (day 7); $t_{(25)} = 4.026$, $p = 0.0002$ (day 10); $t_{(25)} = 2.590$, $p = 0.0307$ (day 14); $t_{(25)} = 5.902$, $p < 0.0001$ (day 28); $t_{(25)} = 3.653$, $p = 0.0010$ (day 35). Hindpaw: $F_{(2,25)} = 165.5$, $p < 0.0001$. Main effect: TBI+vehicle versus sham $t_{(25)} = 17.70$, $p < 0.0001$; TBI+fludarabine versus TBI+vehicle $t_{(25)} = 6.173$, $p < 0.0001$. TBI+fludarabine versus TBI+vehicle on individual day: $t_{(25)} = 3.536$, $p = 0.0015$ (day 3); $t_{(25)} = 4.651$, $p < 0.0001$ (day 5); $t_{(25)} = 3.886$, $p = 0.0004$ (day 7); $t_{(25)} = 4.001$, $p = 0.0003$ (day 10); $t_{(25)} = 4.252$, $p < 0.0001$ (day 28); $t_{(25)} = 2.562$, $p = 0.0332$ (day 35). **F**, Learning: $F_{(2,25)} = 13.08$, $p = 0.0001$. Main effect: TBI+vehicle versus sham $t_{(25)} = 5.096$, $p < 0.0001$; TBI+fludarabine versus TBI+vehicle $t_{(25)} = 3.162$, $p = 0.0122$. TBI+fludarabine versus TBI+vehicle on individual day: $t_{(125)} = 2.759$, $p = 0.0200$ (day 30). One-way ANOVA: $F_{(2,25)} = 1.343$, $p = 0.2793$ (**F**, memory). Data are mean \pm SD. ### $p < 0.001$; TBI versus sham. * $p < 0.05$; ** $p < 0.01$; *** $p < 0.001$; fludarabine versus vehicle control.

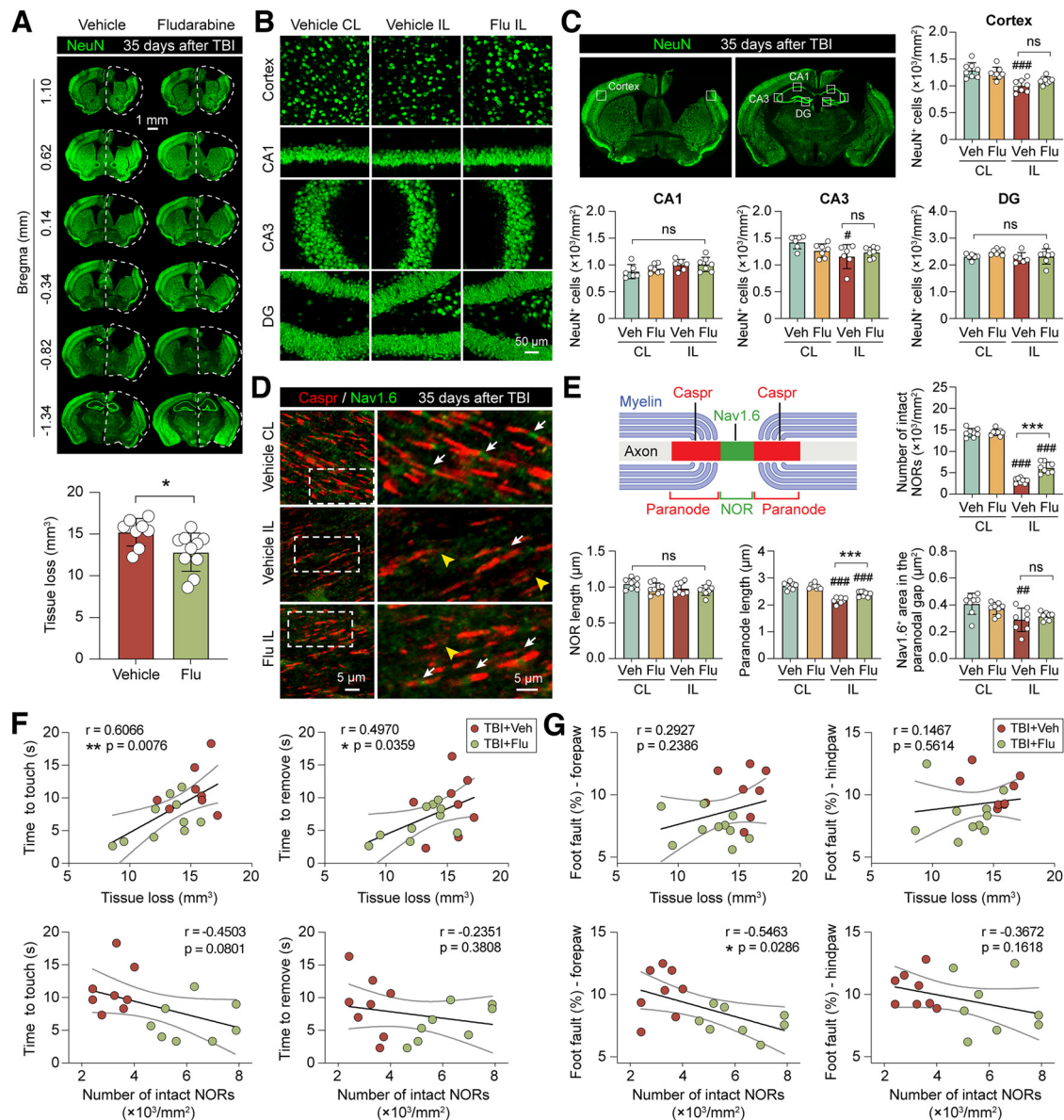


Figure 7. Post-TBI fludarabine treatment elicits sustained improvement of brain integrity. **A–E**, Mice were subjected to TBI and received fludarabine treatment (5 mg/kg) for 5 d. Immunofluorescence staining was performed 35 d after TBI to assess brain injury and white matter integrity. **A**, Tissue loss was assessed on coronal brain sections immunostained for NeuN. $n = 8$ –10 mice per group. Unpaired t test: $t_{(16)} = 2.465$, $p = 0.0254$. **B, C**, The numbers of viable neurons were counted 35 d after TBI in the cortex and hippocampal CA1, CA3, and dentate gyrus (DG) regions on NeuN (green)-immunostained images. Representative images taken from ROIs in **C** are shown in **B**. $n = 6$ –8 mice per group. One-way ANOVA and Bonferroni *post hoc*. Cortex: $F_{(3,28)} = 11.15$, $p < 0.0001$. Veh IL versus CL $t_{(28)} = 5.186$, $p = 0.0001$; Flu IL versus CL $t_{(28)} = 2.471$, $p = 0.1190$; IL Flu versus veh $t_{(28)} = 1.828$, $p = 0.4691$. CA1: $F_{(3,22)} = 1.859$, $p = 0.1661$. CA3: $F_{(3,22)} = 3.431$, $p = 0.0347$. Veh IL versus CL $t_{(22)} = 3.115$, $p = 0.0303$; Flu IL versus CL $t_{(22)} = 0.3761$, $p > 0.9999$; IL Flu versus veh $t_{(22)} = 0.9607$, $p > 0.9999$. DG: $F_{(3,22)} = 1.768$, $p = 0.1827$. **D, E**, The integrity of NORs was assessed by double-label immunostaining of Caspr and Nav1.6 in the CC 35 d after TBI. Shown are representative images (**D**) and summarized data (**E**). Arrow indicates intact NOR. Arrowhead indicates damaged NOR. Rectangle represents the region enlarged in the right column. $n = 8$ mice per group. Number of intact NORs: one-way ANOVA: $F_{(3,28)} = 297.4$, $p < 0.0001$. Bonferroni *post hoc*: Veh IL versus CL $t_{(28)} = 23.70$, $p < 0.0001$; Flu IL versus CL $t_{(28)} = 17.56$, $p < 0.0001$; IL Flu versus veh $t_{(28)} = 6.389$, $p < 0.0001$. NOR length: one-way ANOVA: $F_{(3,28)} = 2.030$, $p = 0.1324$. Paranode length: one-way ANOVA: $F_{(3,28)} = 45.25$, $p < 0.0001$. Bonferroni *post hoc*: Veh IL versus CL $t_{(28)} = 10.02$, $p < 0.0001$; Flu IL versus CL $t_{(28)} = 5.164$, $p = 0.0001$; IL Flu versus veh $t_{(28)} = 4.515$, $p = 0.0006$. Nav1.6⁺ area: one-way ANOVA: $F_{(3,28)} = 5.632$, $p = 0.0038$. Bonferroni *post hoc*: Veh IL versus CL $t_{(28)} = 3.682$, $p = 0.0059$; Flu IL versus CL $t_{(28)} = 1.816$, $p = 0.4808$; IL Flu versus veh $t_{(28)} = 0.7838$, $p > 0.9999$. Data are mean \pm SD. * $p < 0.05$; ** $p < 0.01$; *** $p < 0.001$; IL versus CL. * $p < 0.05$; *** $p < 0.001$ fludarabine versus vehicle. **F, G**, Pearson correlation between the animals' performance in the adhesive removal test (**F**) and foot fault test (**G**), and immunohistochemical parameters representing gross brain tissue loss (top panels) and white matter integrity (number of intact NORs; bottom panels) 35 d after TBI. Lines indicate the fitted equation with 95% CIs.

STAT1 in proinflammatory Mi/M Φ responses *in vivo*, the ablation of which resulted in long-lasting improvement of TBI outcome. Further supporting STAT1 as a legitimate therapeutic target is the remarkable effect of short-term fludarabine treatment in promoting long-term brain integrity and functional recovery after TBI.

Phenotypic heterogeneity of Mi/M Φ in the post-TBI brain has been well established. Regression of early pro-repair “M2”-

like responses and concomitant escalation of proinflammatory “M1”-like responses of Mi/M Φ are thought to underlie the progressive brain damage after TBI (G. Wang et al., 2013; Kumar et al., 2016). Despite the common association of proinflammatory and pro-repair Mi/M Φ phenotypes with deteriorated and improved TBI outcomes, respectively (Pu et al., 2021a; G. Wang et al., 2015), no therapy thus far has actively manipulated Mi/

MΦ phenotype to improve the overall outcome after TBI. The conditional STAT1 mKO mice used in this study are advantageous over conventional KO mice by enabling temporal and cell type-specific control of gene manipulation *in vivo*. STAT1 deletion was induced by tamoxifen treatment at adulthood and only in Mi/MΦ, eliminating potential impact from development and from other types of cells (Durbin et al., 1996). Although we could not rule out functional compensation from other cells on STAT1 deletion in Mi/MΦ, these STAT1 mKO mice are still one of the best tools available to study Mi/MΦ *in vivo*. Since the markers used in this study (e.g., Iba1, Cx3cr1) could not distinguish activated Mi from monocyte-derived MΦ (Witcher et al., 2015), we addressed the role of the entire myeloid cell lineage (Mi and MΦ) together. The emerging new markers that are microglia-specific (e.g., Tmem119) will support future studies to further separate the contribution from Mi versus MΦ. It should be noted that some of these markers may have altered expression under disease conditions (Masuda et al., 2020), and should therefore be validated in the TBI model first for their reliability to label all microglia.

Our combined genetic and pharmacological approaches indicate that STAT1 negatively influences TBI outcome. Our results are consistent with previous correlative findings that reduced STAT1 activation was observed in animals with less injury after TBI (Gao et al., 2020; Sen et al., 2020). On the other hand, several other studies correlated STAT1 function with improved outcome or even the pro-repair “M2”-like Mi/MΦ responses after CNS injuries (Chen et al., 2018; H. Wu et al., 2021). There are several possible explanations to such discrepancies. First, previous studies reported correlative findings on STAT1 and brain injury, rather than directly targeting STAT1 in the context of TBI. Second, previous observations on STAT1 expression were based on whole-brain samples without considering the contribution from different cell types. To this end, STAT1 in other cells could play a synergistic or antagonistic role with STAT1 in Mi/MΦ. Finally, the Mi/MΦ population is highly heterogeneous, and expression of “M1” and “M2” markers is not mutually exclusive. The present study studied Mi/MΦ as one cluster, and future studies may use advanced single-cell analytical tools to further research into the phenotype of Mi/MΦ at single-cell level. As a crucial component of canonical interferon signaling, STAT1’s upstream activators and downstream targets have been well established in the immunology field (Ivashkiv and Donlin, 2014). Therefore, the present study focused on the biological consequence of STAT1 signaling and its systemic impact on the animals’ behavioral performance. Although our study supports a proinflammatory role of STAT1 in the post-TBI brain that is in accordance with its duty in canonical interferon signaling (Ivashkiv and Donlin, 2014), it should be noted that functional dichotomy may exist for this molecule. Interferon-mediated proinflammatory responses could happen without STAT1, when the interferon receptors engage alternative STAT1-independent pathways (Gil et al., 2001). For example, STAT1-null mice have even more severe inflammatory reactions, including leukocyte infiltration and upregulation of proinflammatory cytokines in response to interferon- α ’s presence in the brain (J. Wang et al., 2002), suggesting the complexity of the *in vivo* neuroinflammation milieu. Future studies can further use RNA sequencing to elucidate the genes and networks altered in STAT1-null Mi/MΦ after TBI and reveal context-dependent role of STAT1 signaling *in vivo*.

It is well established that the functional phenotype of Mi/MΦ has profound impact on both cell death and tissue repair/plasticity

in the injured brain. We observed that STAT1 mKO or inhibition drove Mi/MΦ toward the pro-repair “M2”-like phenotype 3–5 d after TBI, an injury stage when Mi/MΦ activation peaks in the mouse CCI model (G. Wang et al., 2013; Kumar et al., 2016), and that both STAT1 mKO and inhibition significantly reduced tissue loss volume and axonal injury 5 d after TBI. Furthermore, “M2”-like Mi/MΦ can be pro-repair, and mitigation of local inflammation also facilitates tissue remodeling by providing a permissive microenvironment (Hu et al., 2015). Although our data support the reduction of early brain injury by STAT1 deletion or inhibition, we could not rule out the possibility that repair processes at the delayed injury stage are also enhanced on STAT1 mKO or inhibition. Future studies examining key repair mechanisms after TBI, such as angiogenesis, oligodendrogenesis, and remyelination with these interventions, would address this limitation of our study.

Both STAT1 mKO and fludarabine promoted long-term functional recovery after TBI, although there were minor differences between these two approaches. For example, fludarabine ameliorated spatial learning deficits in the Morris water maze test (Fig. 6F), whereas STAT1 mKO mice had similar performance compared with WT mice (Fig. 5E). This could be because of fludarabine’s inhibitory effect on STAT1 in other cell types in addition to Mi/MΦ after systemic administration. For example, neuronal STAT1 was shown to contribute to acute cell death in ischemic stroke models (Takagi et al., 2002). Fludarabine could inhibit neuronal STAT1 and offer neuroprotection after TBI, presenting an even better effect than STAT1 mKO. It is noteworthy that fludarabine failed to exert anti-inflammatory effects or improve functional outcome when STAT1 is deleted in Mi/MΦ, as shown in both *in vitro* (Fig. 3F,G) and *in vivo* (Fig. 5A–F) models, suggesting that Mi/MΦ STAT1 is indispensable in fludarabine-afforded effects. Another possible explanation for the different effects between fludarabine treatment and STAT1 mKO is the genetic background of the mice in these two cohorts. The STAT1 mKO mice and matched WT control mice both harbored the Cx3cr1^{CreER} mutation. The resulting Cx3cr1 haploinsufficiency (Parkhurst et al., 2013) could cause the minor outcome difference compared with C56BL/6J mice.

Fludarabine is a purine analog that inhibits DNA synthesis and can easily cross the blood–brain barrier, and is approved by the FDA to treat hematologic malignancies (Johnson et al., 1996). Independent of its incorporation into DNA, fludarabine specifically depletes STAT1 (mRNA and protein) but not other STATs, thereby potentially inhibiting STAT1 (Frank et al., 1999). In our CCI model, fludarabine-treated mice had markedly alleviated neuroinflammation, functional deficits, and brain injury. In addition to these exciting therapeutic effects, there are other reasons supporting the development of fludarabine as a treatment to TBI. First, since fludarabine targets neuroinflammation at the subacute injury stage, its therapeutic time window could be wide. We delivered the first dose of fludarabine at 2 h after TBI, which offers a manageable time window in clinical settings. Future studies may also test whether the administration of fludarabine can be further delayed after the onset of TBI. However, early administration of fludarabine may have additional beneficial effects, such as acute neuroprotection, as discussed above. Secondly, as an FDA-approved chemotherapy drug, fludarabine holds excellent safety and tolerability, especially at the lower doses used here. Our dosage of fludarabine at 5 mg/kg on mice is equivalent to $\sim 15 \text{ mg/m}^2$ in humans (Nair and Jacob, 2016) and is much lower than the recommended dosage for chemotherapy in humans at $25 \text{ mg/m}^2/\text{day}$ (Berlex Canada, 2003). Finally, we used a 5 d transient treatment

regimen, covering the subacute injury stage when neuroinflammation peaks (Kumar and Loane, 2012) but leaving the immune function at the chronic recovery stage intact. Immune cells could participate in post-injury brain repair; normal immune function is also imperative to prevent post-TBI immunodepression and infectious complications (Alharfi et al., 2014; Hazeldine et al., 2015). It should also be noted that fludarabine seemed to exert immunomodulating function instead of indiscriminate suppression of all immune function. A good example is the selective blocking effect of fludarabine on the entry of proinflammatory Ly6C^+ M Φ (Morganti et al., 2015) but not the Ly6C^- patrolling and reparative M Φ (Fig. 2B). Given the aforementioned advantages of fludarabine, future studies are warranted to test its efficacy in subjects at different ages and of both sexes, and in other TBI models such as those modeling a mild TBI (Lynch et al., 2021; L. Wu et al., 2021).

In conclusion, our results demonstrate that STAT1 causatively determines the proinflammatory phenotype of brain M Φ /M Φ after TBI. We are also the first to report that the STAT1 inhibitor fludarabine is a promising treatment to alleviate neuroinflammation and promote long-term functional recovery after TBI.

References

- Alharfi IM, Charyk Stewart T, Al Helali I, Daoud H, Fraser DD (2014) Infection rates, fevers, and associated factors in pediatric severe traumatic brain injury. *J Neurotrauma* 31:452–458.
- Barrett JP, Henry RJ, Shirey KA, Doran SJ, Makarevich OD, Ritzel RM, Meadows VA, Vogel SN, Faden AI, Stoica BA, Loane DJ (2020) Interferon-beta plays a detrimental role in experimental traumatic brain injury by enhancing neuroinflammation that drives chronic neurodegeneration. *J Neurosci* 40:2357–2370.
- Berlex Canada (2003) FLUDARA* product monograph. Pointe-Claire, Quebec.
- Chen S, Ye J, Chen X, Shi J, Wu W, Lin W, Lin W, Li Y, Fu H, Li S (2018) Valproic acid attenuates traumatic spinal cord injury-induced inflammation via STAT1 and NF-kappaB pathway dependent of HDAC3. *J Neuroinflammation* 15:150.
- Durbin JE, Hackenmiller R, Simon MC, Levy DE (1996) Targeted disruption of the mouse Stat1 gene results in compromised innate immunity to viral disease. *Cell* 84:443–450.
- Frank DA, Mahajan S, Ritz J (1999) Fludarabine-induced immunosuppression is associated with inhibition of STAT1 signaling. *Nat Med* 5:444–447.
- Gao C, Yan Y, Chen G, Wang T, Luo C, Zhang M, Chen X, Tao L (2020) Autophagy activation represses pyroptosis through the IL-13 and JAK1/STAT1 pathways in a mouse model of moderate traumatic brain injury. *ACS Chem Neurosci* 11:4231–4239.
- Geissmann F, Manz MG, Jung S, Sieweke MH, Merad M, Ley K (2010) Development of monocytes, macrophages, and dendritic cells. *Science* 327:656–661.
- Gil MP, Bohn E, O'Guin AK, Ramana CV, Levine B, Stark GR, Virgin HW, Schreiber RD (2001) Biologic consequences of Stat1-independent IFN signaling. *Proc Natl Acad Sci USA* 98:6680–6685.
- Hazeldine J, Lord JM, Belli A (2015) Traumatic brain injury and peripheral immune suppression: primer and prospectus. *Front Neurol* 6:235.
- Hu X, Leak RK, Shi Y, Suenaga J, Gao Y, Zheng P, Chen J (2015) Microglial and macrophage polarization—new prospects for brain repair. *Nat Rev Neurol* 11:56–64.
- Ivashkiv LB, Donlin LT (2014) Regulation of type I interferon responses. *Nat Rev Immunol* 14:36–49.
- Johnson S, Smith AG, Loffler H, Osby E, Juliusson G, Emmerich B, Wyld PJ, Hiddemann W (1996) Multicentre prospective randomised trial of fludarabine versus cyclophosphamide, doxorubicin, and prednisone (CAP) for treatment of advanced-stage chronic lymphocytic leukaemia: the French Cooperative Group on CLL. *Lancet* 347:1432–1438.
- Kilkenny C, Browne WJ, Cuthill IC, Emerson M, Altman DG (2010) Improving bioscience research reporting: the ARRIVE guidelines for reporting animal research. *PLoS Biol* 8:e1000412.
- Klover PJ, Muller WJ, Robinson GW, Pfeiffer RM, Yamaji D, Hennighausen L (2010) Loss of STAT1 from mouse mammary epithelium results in an increased Neu-induced tumor burden. *Neoplasia* 12:899–905.
- Kumar A, Alvarez-Croda DM, Stoica BA, Faden AI, Loane DJ (2016) Microglial/macrophage polarization dynamics following traumatic brain injury. *J Neurotrauma* 33:1732–1750.
- Kumar A, Loane DJ (2012) Neuroinflammation after traumatic brain injury: opportunities for therapeutic intervention. *Brain Behav Immun* 26:1191–1201.
- Lawrence T, Natoli G (2011) Transcriptional regulation of macrophage polarization: enabling diversity with identity. *Nat Rev Immunol* 11:750–761.
- Linderman GC, Rachh M, Hoskins JG, Steinerberger S, Kluger Y (2019) Fast interpolation-based t-SNE for improved visualization of single-cell RNA-seq data. *Nat Methods* 16:243–245.
- Liu Y, Li S, Wang R, Pu H, Zhao Y, Ye Q, Shi Y (2021) Inhibition of TGFbeta-activated kinase 1 promotes inflammation-resolving microglial/macrophage responses and recovery after stroke in ovariectomized female mice. *Neurobiol Dis* 151:105257.
- Lynch CE, Eisenbaum M, Algamal M, Balbi M, Ferguson S, Mouzon B, Saltiel N, Ojo J, Diaz-Arrastia R, Mullan M, Crawford F, Bachmeier C (2021) Impairment of cerebrovascular reactivity in response to hypercapnic challenge in a mouse model of repetitive mild traumatic brain injury. *J Cereb Blood Flow Metab* 41:1362–1378.
- Mao L, Yang T, Li X, Lei X, Sun Y, Zhao Y, Zhang W, Gao Y, Sun B, Zhang F (2019) Protective effects of sulforaphane in experimental vascular cognitive impairment: contribution of the Nrf2 pathway. *J Cereb Blood Flow Metab* 39:352–366.
- Marion CM, Radomski KL, Cramer NP, Galdzicki Z, Armstrong RC (2018) Experimental traumatic brain injury identifies distinct early and late phase axonal conduction deficits of white matter pathophysiology, and reveals intervening recovery. *J Neurosci* 38:8723–8736.
- Masuda T, Amann L, Sankowski R, Staszewski O, Errico P, Snaidero N, Costa Jordao MJ, Bottcher C, Kierdorf K, Jung S, Priller J, Misgeld T, Vlachos A, Meyer-Luehmann M, Knobloch KP, Prinz M (2020) Novel Hexb-based tools for studying microglia in the CNS. *Nat Immunol* 21:802–815.
- Morganti JM, Jopson TD, Liu S, Riparip LK, Guandique CK, Gupta N, Ferguson AR, Rosi S (2015) CCR2 antagonism alters brain macrophage polarization and ameliorates cognitive dysfunction induced by traumatic brain injury. *J Neurosci* 35:748–760.
- Nair AB, Jacob S (2016) A simple practice guide for dose conversion between animals and human. *J Basic Clin Pharm* 7:27–31.
- Parkhurst CN, Yang G, Ninan I, Savas JN, Yates JR 3rd, Lafaille JJ, Hempstead BL, Littman DR, Gan WB (2013) Microglia promote learning-dependent synapse formation through brain-derived neurotrophic factor. *Cell* 155:1596–1609.
- Pu H, Ma C, Zhao Y, Wang Y, Zhang W, Miao W, Yu F, Hu X, Shi Y, Leak RK, Hitchens TK, Dixon CE, Bennett MV, Chen J (2021a) Intranasal delivery of interleukin-4 attenuates chronic cognitive deficits via beneficial microglial responses in experimental traumatic brain injury. *J Cereb Blood Flow Metab* 41:2870–2886.
- Pu H, Zheng X, Jiang X, Mu H, Xu F, Zhu W, Ye Q, Jizhang Y, Hitchens TK, Shi Y, Hu X, Leak RK, Dixon CE, Bennett MV, Chen J (2021b) Interleukin-4 improves white matter integrity and functional recovery after murine traumatic brain injury via oligodendroglial PPARgamma. *J Cereb Blood Flow Metab* 41:511–529.
- Reeves TM, Greer JE, Vanderveer AS, Phillips LL (2010) Proteolysis of sub-membrane cytoskeletal proteins ankyrin-G and alphaII-spectrin following diffuse brain injury: a role in white matter vulnerability at nodes of Ranvier. *Brain Pathol* 20:1055–1068.
- Sen T, Saha P, Gupta R, Foley LM, Jiang T, Abakumova OS, Hitchens TK, Sen N (2020) Aberrant ER stress induced neuronal-IFNbeta elicits white matter injury due to microglial activation and T-cell infiltration after TBI. *J Neurosci* 40:424–446.
- Shi L, Rocha M, Zhang W, Jiang M, Li S, Ye Q, Hassan SH, Liu L, Adair MN, Xu J, Luo J, Hu X, Wechsler LR, Chen J, Shi Y (2020) Genome-wide transcriptomic analysis of microglia reveals impaired responses in aged mice after cerebral ischemia. *J Cereb Blood Flow Metab* 40:S49–S66.
- Shi Y, Zhang L, Pu H, Mao L, Hu X, Jiang X, Xu N, Stetler RA, Zhang F, Liu X, Leak RK, Keep RF, Ji X, Chen J (2016) Rapid endothelial cytoskeletal

- reorganization enables early blood–brain barrier disruption and long-term ischaemic reperfusion brain injury. *Nat Commun* 7:10523.
- Stempel M, Kedinger M, Augenlicht L, Klampfer L (2007) Essential role of the JAK/STAT1 signaling pathway in the expression of inducible nitric-oxide synthase in intestinal epithelial cells and its regulation by butyrate. *J Biol Chem* 282:9797–9804.
- Takagi Y, Harada J, Chiarugi A, Moskowitz MA (2002) STAT1 is activated in neurons after ischemia and contributes to ischemic brain injury. *J Cereb Blood Flow Metab* 22:1311–1318.
- Wang G, Zhang J, Hu X, Zhang L, Mao L, Jiang X, Liou AK, Leak RK, Gao Y, Chen J (2013) Microglia/macrophage polarization dynamics in white matter after traumatic brain injury. *J Cereb Blood Flow Metab* 33:1864–1874.
- Wang G, Shi Y, Jiang X, Leak RK, Hu X, Wu Y, Pu H, Li WW, Tang B, Wang Y, Gao Y, Zheng P, Bennett MV, Chen J (2015) HDAC inhibition prevents white matter injury by modulating microglia/macrophage polarization through the GSK3 β /PTEN/Akt axis. *Proc Natl Acad Sci USA* 112:2853–2858.
- Wang J, Schreiber RD, Campbell IL (2002) STAT1 deficiency unexpectedly and markedly exacerbates the pathophysiological actions of IFN- α in the central nervous system. *Proc Natl Acad Sci USA* 99:16209–16214.
- Wang R, Liu Y, Ye Q, Hassan SH, Zhao J, Li S, Hu X, Leak RK, Rocha M, Wechsler LR, Chen J, Shi Y (2020a) RNA sequencing reveals novel macrophage transcriptome favoring neurovascular plasticity after ischemic stroke. *J Cereb Blood Flow Metab* 40:720–738.
- Wang R, Pu H, Ye Q, Jiang M, Chen J, Zhao J, Li S, Liu Y, Hu X, Rocha M, Jadhav AP, Chen J, Shi Y (2020b) Transforming growth factor β -activated kinase 1-dependent microglial and macrophage responses aggravate long-term outcomes after ischemic stroke. *Stroke* 51:975–985.
- Witcher KG, Bray CE, Chunhai T, Zhao F, O'Neil SM, Gordillo AJ, Campbell WA, McKim DB, Liu X, Dziabis JE, Quan N, Eiferman DS, Fischer AJ, Kokiko-Cochran ON, Askwith C, Godbout JP (2021) Traumatic brain injury causes chronic cortical inflammation and neuronal dysfunction mediated by microglia. *J Neurosci* 41:1597–1616.
- Witcher KG, Eiferman DS, Godbout JP (2015) Priming the inflammatory pump of the CNS after traumatic brain injury. *Trends Neurosci* 38:609–620.
- Wu H, Zheng J, Xu S, Fang Y, Wu Y, Zeng J, Shao A, Shi L, Lu J, Mei S, Wang X, Guo X, Wang Y, Zhao Z, Zhang J (2021) Mer regulates microglial/macrophage M1/M2 polarization and alleviates neuroinflammation following traumatic brain injury. *J Neuroinflammation* 18:2.
- Wu L, Chan ST, Edmiston WJ 3rd, Jin G, Levy ES, Kwong KK, Mannix R, Meehan WP, Chifamba FF, Lipton JO, Whalen MJ, Chen YI (2021) Persistent CO₂ reactivity deficits are associated with neurological dysfunction up to one year after repetitive mild closed head injury in adolescent mice. *J Cereb Blood Flow Metab* 41:3260–3272.
- Xia Y, Pu H, Leak RK, Shi Y, Mu H, Hu X, Lu Z, Foley LM, Hitchens TK, Dixon CE, Bennett MVL, Chen J (2018) Tissue plasminogen activator promotes white matter integrity and functional recovery in a murine model of traumatic brain injury. *Proc Natl Acad Sci USA* 115:E9230–E9238.